New Phytologist

Research

Heme catabolism mediated by heme oxygenase in uninfected interstitial cells enables efficient symbiotic nitrogen fixation in *Lotus japonicus* nodules

Yu Zhou[1], Longlong Wang[1], Maria Carmen Rubio[2], Carmen Pérez-Rontomé[2], Yumiao Zhou[1], Yongmei Qi[1], Tao Tian[1], Weiqing Zhang[1], Qiuling Fan[1], Manuel Becana[2] and Deqiang Duanmu[1,3]

[1]National Key Laboratory of Agricultural Microbiology, Hubei Hongshan Laboratory, Shenzhen Institute of Nutrition and Health, Huazhong Agricultural University, Wuhan 430070, China; [2]Departamento de Biología Vegetal, Estación Experimental de Aula Dei, Consejo Superior de Investigaciones Científicas, Avenida Montañana 1005, Zaragoza 50059, Spain; [3]Shenzhen Branch, Guangdong Laboratory for Lingnan Modern Agriculture, Genome Analysis Laboratory of the Ministry of Agriculture, Agricultural Genomics Institute at Shenzhen, Chinese Academy of Agricultural Sciences, Shenzhen 518000, China

Author for correspondence:
Deqiang Duanmu
Email: duanmu@mail.hzau.edu.cn

Received: *24 January 2023*
Accepted: *19 May 2023*

New Phytologist (2023) **239:** 1989–2006
doi: 10.1111/nph.19074

Key words: heme homeostasis, heme oxygenase, leghemoglobin, *Lotus japonicus*, nodule senescence, symbiotic nitrogen fixation.

Summary

- Legume nodules produce large quantities of heme required for the synthesis of leghemoglobin (Lb) and other hemoproteins. Despite the crucial function of Lb in nitrogen fixation and the toxicity of free heme, the mechanisms of heme homeostasis remain elusive.
- Biochemical, cellular, and genetic approaches were used to study the role of heme oxygenases (HOs) in heme degradation in the model legume *Lotus japonicus*. Heme and biliverdin were quantified and localized, HOs were characterized, and knockout *LORE1* and CRISPR/Cas9 mutants for LjHO1 were generated and phenotyped.
- We show that LjHO1, but not the LjHO2 isoform, is responsible for heme catabolism in nodules and identify biliverdin as the *in vivo* product of the enzyme in senescing green nodules. Spatiotemporal expression analysis revealed that *LjHO1* expression and biliverdin production are restricted to the plastids of uninfected interstitial cells. The nodules of *ho1* mutants showed decreased nitrogen fixation, and the development of brown, rather than green, nodules during senescence. Increased superoxide production was observed in *ho1* nodules, underscoring the importance of LjHO1 in antioxidant defense.
- We conclude that LjHO1 plays an essential role in degradation of Lb heme, uncovering a novel function of nodule plastids and uninfected interstitial cells in nitrogen fixation.

Introduction

Leguminous plants are able to establish symbiotic associations with soil bacteria collectively known as rhizobia. As a result of a molecular dialog between the two partners, a new symbiotic organ, the nodule, is formed on the roots (Roy *et al.*, 2020). In the nodules, bacteria differentiate into bacteroids that express the enzyme complex nitrogenase that fixes atmospheric nitrogen. This process is called symbiotic nitrogen fixation (SNF) and provides a sustainable source of nitrogen to natural and agricultural ecosystems (Lindström & Mousavi, 2020; Roy *et al.*, 2020). Nitrogenase is rapidly and irreversibly inactivated by O_2, which is therefore kept at low levels around the bacteroids; however, bacteroids have a high respiratory demand of O_2 to produce energy and fix nitrogen. To solve this O_2 paradox, legumes have an O_2 diffusion barrier located mainly in the inner cortex of nodules, along with a high concentration of leghemoglobin (Lb) in the cytosol of infected cells (IC). This hemoprotein binds O_2 reversibly and with high affinity so that the free O_2 concentration in IC is only *c.* 3–28 nM (Becana & Klucas, 1992; Hunt & Layzell, 1993).

Legume genomes typically encode multiple *Lb* genes (for a recent review, see Larrainzar *et al.*, 2020). The *in vivo* function of Lbs in maintaining an efficient SNF was demonstrated in the model legume *Lotus japonicus*, which encodes three *Lb* genes. Plants of *L. japonicus* with transient suppression of *Lb* transcripts by RNA interference exhibited small white nodules, with a *c.* 2.5-fold increase in internal free O_2 concentration and alterations in the expression of many SNF-related genes, including bacterial *nif* and *fix* genes (Ott *et al.*, 2005, 2009). Stable knockout mutants with all three *Lbs* disrupted by CRISPR/Cas9 showed SNF defects and premature nodule senescence, with enhanced accumulation of reactive oxygen species (ROS) in the host cells (Wang *et al.*, 2019). The regulation of *Lb* gene expression in nodules has been linked to the activity of NIN (Nodule Inception) and NIN-like protein (NLP) transcription factors (Jiang *et al.*, 2021).

Functional Lbs contain the majority of nodule heme and account for 25–30% of the total soluble protein of mature

nodules (Baulcombe & Verma, 1978). Thus, the rate of heme biosynthesis needs to be very high to meet the demands of Lbs and other nodule hemoproteins. Despite heme being critical in all living organisms, the concentration of intracellular free heme (unbound to proteins) must be controlled precisely to minimize its toxic effects that may originate from ROS production and lipid peroxidation (Anzaldi & Skaar, 2010; Chiabrando *et al.*, 2014). The half-life of Lbs was estimated to be *c.* 2 d in soybean mature nodules (Bisseling *et al.*, 1980). The content of Lb is dramatically reduced in aging or stress-induced senescent nodules (Matamoros *et al.*, 1999; Puppo *et al.*, 2005; Dhanushkodi *et al.*, 2018; Du *et al.*, 2020). Heme released from Lbs in mature and senescent nodules could lead to lipid peroxidation and degradation of the symbiosome membrane (Herrada *et al.*, 1993). In *L. japonicus*, the absence of Lbs in the triple mutant (*lb123*) resulted in a significant disruption of mitochondrial cristae, which might be related to mis-accumulation of free heme in the mutant nodules (Wang *et al.*, 2019). However, the mechanisms of heme homeostasis in legume nodules remain largely unexplored.

The enzymatic catabolism of heme in microorganisms, animals, and plants is mediated by heme oxygenase (HO), IsdG family protein, cytoplasmic heme-binding protein ChuS/PhuS, and the SAM superfamily protein ChuW (Suits *et al.*, 2005; Shekhawat & Verma, 2010; Lee *et al.*, 2014; LaMattina *et al.*, 2016). HO is the dominant or even the only heme-degrading enzyme present in plants and animals, where it catalyzes the conversion of heme to biliverdin (BV), ferrous iron (Fe^{2+}), and carbon monoxide (CO). In mammals, HO catalyzes heme degradation during the breakdown of hemoglobin (Korolnek & Hamza, 2015). In cyanobacteria, eukaryotic algae, and higher plants, BV can be further reduced to various types of bilins, which act as the prosthetic group of phytochrome or phycobiliprotein and are therefore essential for light signaling or light harvesting in those phototrophs (Legris *et al.*, 2019; Adir *et al.*, 2020; Villafani *et al.*, 2020). Plant HO also functions in the tolerance of oxidative stress triggered by environmental cues such as high salinity and heavy metals (Balestrasse *et al.*, 2008; Shen *et al.*, 2011). The absence of HO impairs the acquisition and reutilization of heme iron in *Chlamydomonas reinhardtii* (Duanmu *et al.*, 2013). Overall, HO is a key enzyme with multifaceted roles in regulating various biological processes, including photosynthesis, antioxidant defense, and heme homeostasis (Mahawar & Shekhawat, 2018).

The present study was undertaken to explore the biological function of HO in regulating heme homeostasis and SNF in *L. japonicus* nodules. We show that the green nodules (GN) formed during developmental or stress-induced senescence contain abundant BV and that this green bile pigment is produced from heme degradation by heme oxygenase 1 (LjHO1) but not by the LjHO2 isoform. Spatiotemporal expression analysis revealed that *LjHO1* expression is restricted to the uninfected interstitial cells (UC) of nodules, which was an unexpected finding because IC contain large amounts of Lbs and heme. Consistent with the plastid localization of LjHO1, BV accumulates in the plastids of UC. Knockout of *LjHO1* by CRISPR/Cas9 resulted in a reduced SNF of mature nodules and in the disappearance of GN and the formation of brown nodules (BN) in senescent nodules. An increased superoxide level was observed in *ho1* mutant nodules, underscoring the importance of LjHO1 in antioxidant defense against environmental stress. We conclude that LjHO1 in the plastids of UC plays an essential role in Lb-heme degradation and in maintaining an efficient SNF in *L. japonicus* nodules.

Materials and Methods

Plant materials and growth conditions

Lotus japonicus ecotypes MG-20 and Gifu B-129 were used as wild-type (WT) plants in this study. The *ho1-1* and *ho1-2* mutants were generated in MG-20 background using CRISPR/Cas9, whereas *ho1-3* (line 30070968) and *ho1-4* (line 30128287) mutants are in Gifu background and were obtained from the Lotus Base (https://lotus.au.dk/). Surface-disinfected seeds were germinated on half-strength Murashige and Skoog medium for 2 d in the dark and were transferred to a growth chamber at 24°C with a 16 h : 8 h, light : dark cycle and light fluence rate of *c.* 120 μmol photons m^{-2} s^{-1}. After growing under light for 5 d, seedlings were transferred to pots containing sterile perlite : vermiculite (1 : 3) in a growth chamber as indicated before and were grown for another 7 d before inoculation with *Mesorhizobium loti* MAFF303099 (Kaneko *et al.*, 2000) or rhizobial mutants lacking heme-degrading enzymes. Plants were grown until harvest with half-strength B&D solution containing 0.5 mM KNO_3 (Broughton & Dilworth, 1971). For nitrate treatment, plants at 4 wk post-inoculation (wpi) were treated with 20 mM KNO_3 on the first and third days during the 5-d treatment. For the continuous darkness treatment, plants at 4 wpi were fully shaded for 5 d.

Knockout of LjHO1 by CRISPR/Cas9

CRISPR/Cas9 gene editing was conducted as previously described (L.X. Wang *et al.*, 2016). Briefly, two guide RNAs (gRNAs) were designed using the gRNA design tool (http://cbi.hzau.edu.cn/crispr/; Lei *et al.*, 2014) and cloned into the pBlueScript SK+-LjU6-sgRNA vector. The two resulting LjU6-gRNA1-sgRNA and LjU6-gRNA2-sgRNA fragments were ligated and cloned into the pCAMBIA1300-35S:Cas9 binary vector (L.X. Wang *et al.*, 2016). The final vector was introduced into MG-20 via *Agrobacterium tumefaciens* EHA105-mediated stable transformation. Two independent homozygous mutants (*ho1-1* and *ho1-2*) were obtained and their SNF phenotypes were analyzed in T2 plants.

Construction of rhizobial mutants

A two-step homologous recombination approach was used to generate markerless target gene deletion. Flanking sequences of target genes were cloned into pK18mobsacB (Schafer *et al.*, 1994) and were transformed into *M. loti* MAFF303099 by mating with *Escherichia coli* S17-1. Colonies were selected using TY medium containing fosfomycin and kanamycin. The positive colonies were

used for detection of site-specific integration. Mutation of *HmuS* was introduced into the HmuQ$^-$ mutant to yield the HmuQ$^-$ HmuS$^-$ double mutant, and the HmuQ$^-$ HmuS$^-$ HemW$^-$ triple mutant was obtained by introducing *HemW*$^-$ mutation into HmuQ$^-$ HmuS$^-$ recipient cells. Detailed procedures are described in Supporting Information Methods S1.

Plant hairy root and stable transformations

Hairy root and stable transformations of *L. japonicus* MG-20 or Gifu B-129 were performed using protocols described previously (Wang *et al.*, 2019). For hairy root transformation, *A. rhizogenes* LBA1334 harboring corresponding vectors was used and plants with transgenic roots were identified by GFP or mCherry fluorescence with a fluorescence stereo-microscope. For stable transformation, *A. tumefaciens* EHA105 was used. The T_1 plants of homozygous and Cas9-free mutants were allowed to self-cross to produce T_2 seeds (L.X. Wang *et al.*, 2016). Phenotypic analyses were performed using T_2 plants or progeny plants derived from T_2.

Lotus japonicus grafting

Lotus japonicus seeds were germinated and seedlings were grown inversely on half-strength MS medium for 36 h in darkness. Seedlings with elongated radicle were switched to vertical growth for 5 d at 24°C in a 16 h : 8 h, light : dark regime. For shoot–root grafting, the seedlings were cut perpendicularly where chlorophyll begins to deposit (*c.* 0.5 cm below the cotyledons). A sterile polyethylene tube with a length of 0.5 cm and a diameter of 0.8 mm was placed on the root and the stems of other plants were inserted into the tube to ensure that the incisions between the stem and the root were in close contact. The parts below the cotyledons of grafted seedlings were covered with sterilized filter paper and cultured at 24°C in a 16 h : 8 h, light : dark cycle. After 2 wk, grafted seedlings were transferred to vermiculite and watered with B&D nutrient solution in a growth chamber. Symbiotic phenotypes were analyzed at 4 wpi.

HO activity assay

Heme oxygenase enzymatic activity was determined by monitoring the formation of bilirubin (BR) as previously described (Duanmu *et al.*, 2013) with the following modifications. The reaction mixture contained 0.1 M HEPES (pH 7.2), 0.15 mg ml^{-1} BSA, 2 mM iron chelator Tiron, 5 mM ascorbate, 50 units ml^{-1} catalase, 5 μM ferredoxin, 0.025 units ml^{-1} ferredoxin-NADP$^+$ reductase (FNR), 200 nM recombinant biliverdin reductase (GST-BVR), and 1 μM GST-LjHO1ΔTP (or GST-LjHO2ΔTP, or GST control). Hemin was added into the solution at a final concentration of 10 μM to ensure a protein-to-heme ratio of *c.* 1 : 10. After incubation at room temperature for 5 min, the reaction was initiated by the addition of an NADPH regeneration system consisting of 3.2 mM glucose 6-phosphate, 0.4 mM NADP$^+$, and 3 units ml^{-1} yeast glucose 6-phosphate dehydrogenase. The reaction mixture was quickly inverted a few times in a cuvette and the absorbance changes of the mixture between 350 and 800 nm were recorded up to 36 min at 6 min intervals.

Protein subcellular localization

To examine the subcellular localization of LjHO1 and LjHO2 in Arabidopsis protoplasts, the full-length coding sequences of LjHO1 and LjHO2 were amplified from a cDNA library and cloned into the pM999-35S:YFP vector for expression of YFP fusion proteins. The resulting vectors (pM999-35S:LjHO1-YFP and pM999-35S:LjHO2-YFP) and the control construct (pM999-35S:YFP) were, respectively, introduced into Arabidopsis protoplasts using the polyethylene glycol method, as described previously (Yoo *et al.*, 2007). To investigate the subcellular localization of LjHO1 in *L. japonicus* nodules, the full-length coding sequence of LjHO1 was fused to green fluorescent protein (sGFP, bearing the S65T mutation) and cloned into the pCAMBIA1300 binary vector. The 35S promoter was replaced by the *LjHO1* native promoter (*c.* 2.9 kb) and the resulting vector (pCAMBIA1300-pLjHO1:LjHO1-sGFP) was used for hairy root transformation into MG-20. Transgenic plants were inoculated with mCherry-labeled *M. loti* MAFF303099. Nodules at 4 wpi were sectioned and visualized under a confocal laser scanning microscope (SP8 TCS; Leica, Wetzlar, Germany).

GUS staining

Expression patterns of the 2.9-kb promoter region of *LjHO1* and the 2.1-kb promoter region of *LjHO2* were analyzed by GUS staining. Promoter fragments were cloned into either DX2181G-Hyg or DX2181G-mCherry vectors. The resulting plasmids were, respectively, used for stable transformation via *A. tumefaciens* (pLjHO1:GUS) or hairy root transformation via *A. rhizogenes* (pLjHO2:GUS). Nodules of transformed plants at 4 or 6 wpi were used for GUS staining. Detailed information is given in Methods S1.

Determination of heme and biliverdin by UPLC-MS/MS

Contents of heme and BV in nodules were determined by ultra-performance liquid chromatography/tandem mass spectrometry (UPLC-MS/MS). Nodules were ground to a fine powder in liquid nitrogen. Then, 0.2 ml of acetonitrile–acetic acid (v/v, 4 : 1) was added and the tubes were vortexed for 1 min. After centrifugation for 10 min at 12 000 ***g***, the supernatant was transferred to new tubes and maintained on ice in the dark until use. A reversed phase C_{18} column was used and a gradient elution program using 0.03% (v/v) formic acid aqueous solution (solvent A) and acetonitrile (solvent B) as mobile phase was applied. The detection wavelengths of heme and BV were 400 and 377 nm, respectively. Quantitative calculations were carried out by comparing the corrected peak area ratios of analytes with the peak area of the heme or BV standards. Detailed information is given in Methods S1.

Biliverdin sensor

The fluorescent BV sensor iBlueberry (Yu *et al.*, 2016) was used to estimate BV production in nodules. The coding sequence of iBlueberry was fused to the 3 × FLAG tag and was cloned into the pUB-GFP binary vector using the *Bam*HI/*Kpn*I sites. For plastid targeting, the transit peptide of LjHO1 (amino acids 1–56) was fused to the N-terminus of iBlueberry via *Xba*I/*Bam*HI sites. Expression of iBlueberry was driven by the *LjUBQ1* promoter. The final vector was used for hairy root transformation into MG-20 and *ho1-1* mutant, or into Gifu and *ho1-3* mutant. Nodules of transformed plants at 6 wpi were sectioned (80–100 µm thickness) and the BV-chromophorylated iBlueberry signal was acquired with excitation at 644 nm and an emission peak at 667 nm using a TCS SP8 STED microscope (Leica).

Immunogold localization of Lb

For immunogold electron microscopy, nodules were fixed and processed using high pressure freezing and low temperature embedding in Lowicryl HM23 resin (Polysciences, Bergstrasse, Germany) as previously described (Rubio *et al.*, 2009). Sections were incubated in 15-nm gold particles conjugated to protein A for 1 h. The immunogold-labeled sections were viewed and digitally photographed using a JEM 1400 transmission electron microscope (JEOL, Hertfordshire, UK). As negative controls, serial sections were immunogold labeled with non-immune serum (diluted 1 : 5) substituted for the primary antibody.

Superoxide and hydrogen peroxide detection

Superoxide was detected using nitroblue tetrazolium (NBT) staining. Nodules were sectioned (*c.* 85 µm thickness) and immersed in staining buffer (50 mM potassium phosphate, pH 7.8, 0.25 mM NBT; Sigma-Aldrich) for 1 h at room temperature in the dark. For the detection of H_2O_2, nodule sections were stained with 3,3′-diaminobenzidine (DAB; Sigma-Aldrich) buffer (10 mM Tris-HCl, pH 7.4, 1 mg ml^{-1} DAB) for 5 min in the dark at room temperature. To test ROS inhibitors and scavengers, nodule sections were preincubated for 1 h in the dark and then subjected to the same staining protocol as described above. Specifically, we examined the effect of 100 µM diphenyleneiodonium (DPI; Sigma-Aldrich) on NBT staining and the effects of 1 mM KCN, 10 mM ascorbate, or 10 mM KI on DAB staining. DPI is an inhibitor of NADPH oxidase, KCN inhibits the endogenous peroxidase on which the DAB reaction is based, and KI and ascorbate are H_2O_2 scavengers (Dunand *et al.*, 2007; Sandalio *et al.*, 2008). Images were acquired using a light microscope (DM750; Leica).

Analysis of melanin-like pigments

Melanin-like pigments were analyzed following a published method (Shoeva *et al.*, 2020). Nodules (*c.* 100 mg) were ground into a fine powder in liquid nitrogen and resuspended in 1.0 ml of 1 M NaOH. After centrifugation at 12 000 ***g*** for 10 min, the supernatant was transferred to a new centrifuge tube and the pH of the supernatant was adjusted to *c.* 2.0 with 12 M HCl. After a second centrifugation at 12 000 ***g*** for 10 min, the pellet was washed twice with distilled water and redissolved in 100 µl 0.1 M NaOH. Oxidizing agents, including 30% H_2O_2, 0.1 M $KMnO_4$, or 1.0 mg ml^{-1} $FeCl_3$, were added to the solution (v/v, 1 : 10) to compare the redox properties.

Expression and purification of recombinant proteins

Coding sequences of LjHO1ΔTP (amino acids 57–282) and LjHO2ΔTP (amino acids 47–265) were cloned into the pGEX-6P-1 vector. The resulting vectors were introduced into *E. coli* BL21 (DE3). The expression of GST-LjHO1ΔTP and GST-BVR was induced with 0.5 mM isopropyl β-D-1-thiogalactopyranoside (IPTG) for 6 h at 28°C, whereas GST-LjHO2ΔTP expression was induced with 0.3 mM IPTG at 16°C overnight. GST-fusion proteins were purified with GST resin (GenScript, Nanjing, China). Details are given in Methods S1.

Quantitative real-time PCR

Total RNA was extracted from nodules using Trizol reagent (Thermo Fisher Scientific, Carlsbad, CA, USA). Quantitative real-time PCR (qRT-PCR) analyses were performed using the KAPA SYBR FAST qPCR Master Mix reagent (KAPA Biosystems, Shanghai, China). PCRs were carried out with the LightCycler 480 Instrument (Roche). Data were normalized against the endogenous gene *LjUBQ1* (Lj5g3v2060710). All reactions were performed with three biological replicates. Primers used for qRT-PCR are provided in Table S1.

Nitrogenase activity measurement by the acetylene reduction assay

Nodule nitrogen fixation was estimated as acetylene reduction activity (Wang *et al.*, 2019). Briefly, nodulated roots or specific types of nodules were collected and placed in 30 ml glass vials with rubber caps. Acetylene (2 ml) was injected into the vial and, after incubation at 28°C for 2 h, the amount of ethylene was determined by gas chromatography using a GC-4000A gas chromatograph (East & West Analytical Instruments, Beijing, China).

Statistical analysis

Student's *t*-test and Tukey's multiple comparison test were used where appropriate. Bar graphs were prepared using Prism 8 (GraphPad Software, Boston, MA, USA).

Results

Biliverdin is produced in senescent green nodules

The change in nodule color is one of the most significant morphological features of nodule senescence. In *L. japonicus*, the

nodule color gradually changed during developmental senescence (aging) from red (4 wpi) to green (8 wpi). Also, nodules at 4 wpi exhibited dramatic color changes when senescence was induced after treatment of plants with excess nitrate or by exposing them to continuous darkness (Fig. 1a). Degradation of Lb may account for the disappearance of the red color in senescent nodules. The heme of Lb may be converted into a green bile pigment, BV, at least *in vitro*, by the so-called 'coupled oxidation' of Lb with ascorbate in the presence of O_2 (Lehtovaara & Pertiläa, 1978). However, the conversion of Lb heme into BV has not been proven to occur *in vivo* in legume nodules. Consequently, as a preliminary step of our study, we determined by UPLC-MS/MS the relative contents of heme and BV in red nodules (RN) at 4 wpi and compared them with those of GN formed under various conditions (Figs 1b,c, S1). Our results show that heme is highly abundant in RN and decreases drastically in GN of plants supplied with 20 mM KNO_3 (*c.* 85%) or exposed to prolonged darkness (*c.* 93%), as well as in aging nodules at 8 wpi (*c.* 75%; Figs 1b, S1). In parallel, the amounts of BV increased by *c.* 31-, 88-, and 9-fold in these three types of GN compared with RN (Figs 1c, S1). We thus conclude that formation of GN is associated with heme degradation and BV accumulation.

LjHO1 converts heme into biliverdin

The enzyme-mediated catabolism of heme in photosynthetic tissues of higher plants is typically performed by HO (Mahawar & Shekhawat, 2018), yielding BV, CO, and Fe^{2+} (Fig. 1d). Consequently, the second step of our study was to determine whether this reaction takes place in nodules. To identify the specific *HO* genes in *L. japonicus*, we performed BLAST searches in three Lotus genome databases (Gifu v.1.2, MG-20 v.3.0, and MG-20 HAU Lj1.0) using four Arabidopsis HOs (AtHO1/2/3/4) as queries. Two HOs were identified and found to be grouped into two families by phylogenetic tree analysis (Fig. 2a). These two *L. japonicus* HOs were, respectively, named LjHO1 (Lj1g3v0672150) and LjHO2 (Lj5g0008202). HO enzymatic activity was compared *in vitro* using a mammalian biliverdin reductase as the coupling enzyme, which reduces BV to bilirubin (BR). Recombinant LjHO1 fusion protein with the GST-tag and without the predicted chloroplast transit peptide (GST-LjHO1ΔTP) exhibited heme degrading activity, as evidenced by an absorbance increase at *c.* 450 nm (BR formation) and an absorbance decrease at *c.* 405 nm (heme consumption). By contrast, negligible changes were observed in the reaction mixture containing GST control or GST-LjHO2ΔTP (Fig. 2b–d). The absence of HO activity for LjHO2 is consistent with the lack of the conserved histidine residue that is essential for heme iron binding and heme cleavage (Fig. S2; Gisk *et al.*, 2010; Shekhawat & Verma, 2010). Therefore, LjHO1, but not LjHO2, is a *bona fide* HO in *L. japonicus*.

LjHO1 is localized to the plastids of uninfected interstitial cells

To identify the *HO* genes related to SNF, qRT-PCR and immunoblot analyses were performed to detect the expression profiles of *LjHOs* in different tissues of *L. japonicus* plants. *LjHO1* transcript and protein were highly accumulated in mature nodules (4 wpi) and showed relatively higher levels of expression in leaves compared to roots and shoots (Fig. 3a,b). By contrast, the expression level of *LjHO2* was not apparently higher in nodules (Fig. S3a). To investigate the expression pattern of *LjHOs* during SNF, we analyzed the changes in transcript abundance of *LjHO1* and *LjHO2* in uninoculated roots (0 wpi) and nodules (1–10 wpi), spanning the whole nodule development from initiation to senescence. The *LjHO1* mRNA level was upregulated during nodule maturation at 2 wpi and in mature nodules at 4 and 6 wpi, and was dramatically increased by *c.* 20-fold in senescent nodules at 8 and 10 wpi (Fig. 3c). Immunoblot analysis confirmed that the LjHO1 protein was abundant in mature nodules (4 and 6 wpi) and further increased in senescent nodules (8 and 10 wpi; Fig. 3d). By contrast, the transcript level of *LjHO2* did not significantly increase during nodule development (Fig. S3b).

We next performed a promoter-GUS fusion experiment using *c.* 2.9 and 2.1 kb promoter fragments of *LjHO1* and *LjHO2*, respectively. GUS staining of stably transformed *L. japonicus* plants showed that the *LjHO1* promoter was activated in mature nodules at 4 and 6 wpi, and that the signal was restricted to UC rather than IC (Fig. 3e,f), where heme synthesis is in much greater demand due to the abundant heme-containing Lbs. By contrast, the *LjHO2* promoter exhibited activity only in vascular bundles of roots and mature nodules, but was absent from UC or IC (Fig. S3c).

Plant HOs contain chloroplast transit peptides and are located to the chloroplasts of photosynthetic tissues and to the plastids of root cells (Muramoto *et al.*, 1999; Gisk *et al.*, 2010; Shekhawat & Verma, 2010). To confirm the subcellular localization of LjHOs, LjHO1-YFP and LjHO2-YFP fusion proteins were transiently expressed in Arabidopsis protoplasts under the control of the 35S promoter. Fluorescence signals of two fusion proteins were co-localized with chlorophyll autofluorescence, unlike the cytosolic localization of the YFP control, suggesting that both LjHO1 and LjHO2 are located to the chloroplasts (Figs 3g, S3d). The localization of LjHO1 was further examined in hairy-root transformed *L. japonicus* plants by expressing LjHO1-sGFP fusion protein under the control of its native promoter. In 4 wpi nodules, the LjHO1-sGFP fluorescence signal was observed in the plastids of UC but was completely absent from IC (Fig. 3h). These data indicate that LjHO1 functions in heme degradation in the plastids of UC in *L. japonicus* nodules.

The *ho1* mutant nodules show reduced SNF and accumulation of brown pigments

To gain genetic insight into the biological function of LjHO1 in SNF, we generated two *ho1* mutants in MG-20 background using CRISPR/Cas9 (L.X. Wang *et al.*, 2016). The *ho1-1* mutant carries a 267-bp deletion with a 1-bp insertion in exon 1, while the *ho1-2* mutant carries a 281-bp deletion (Fig. S4a). The LjHO1 protein was undetectable in nodules of *ho1-1* and *ho1-2* plants, indicating that both are null mutants (Fig. S4b). In addition, the transcript abundance of *LjHO2* shows no significant differences in *ho1-1*

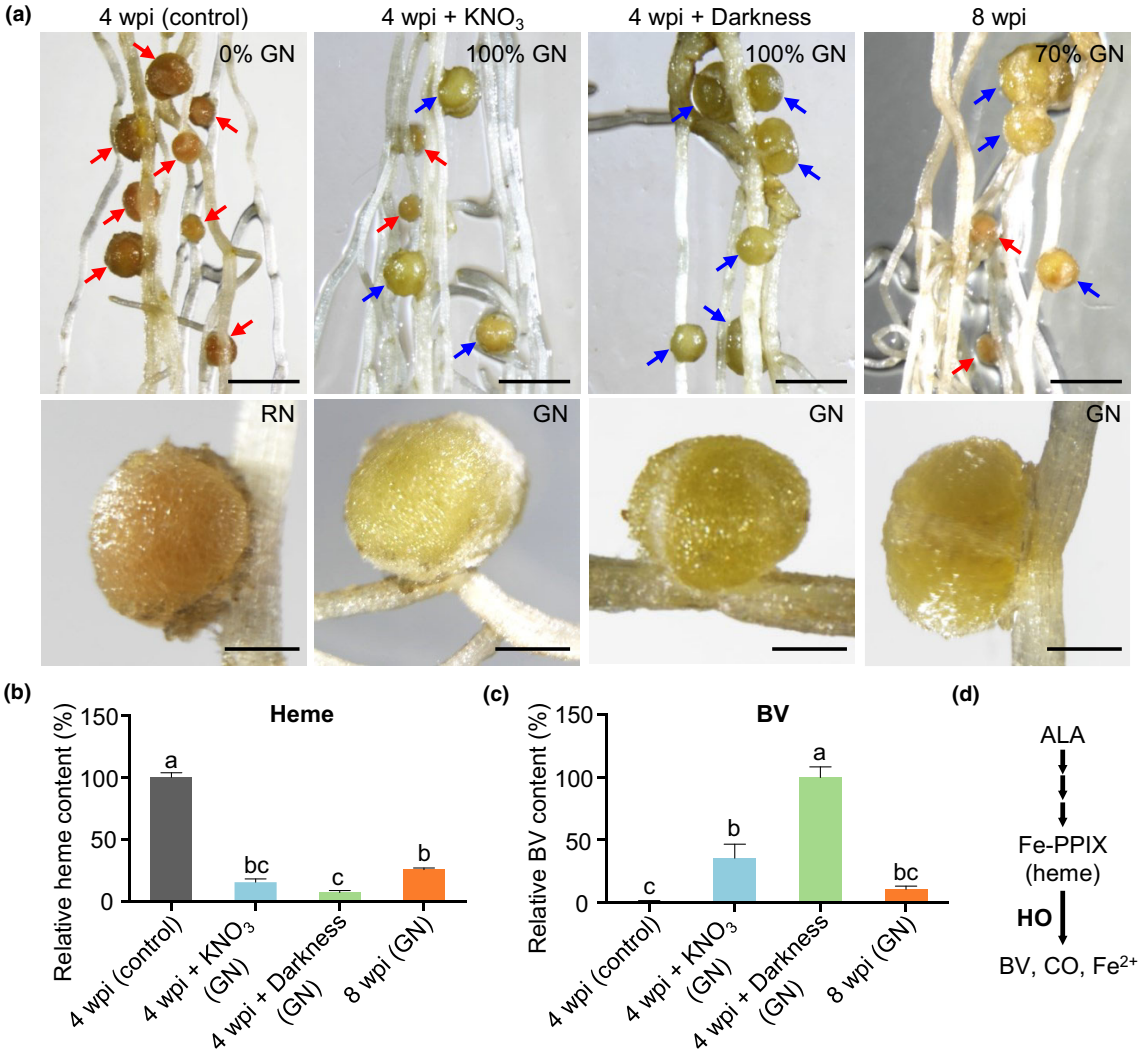

Fig. 1 Biliverdin (BV) accumulates in senescent nodules. (a) Phenotype of *Lotus japonicus* MG-20 mature nodules at 4 wk post-inoculation (wpi), developmentally senescent (8 wpi) nodules, or nodules under stress conditions (upper panel). High-resolution images of representative red nodules (RN) and green nodules (GN) are shown (lower panel). For stress treatments, 5-d-old seedlings were inoculated with *Mesorhizobium loti* MAFF303099 and then plants at 4 wpi were treated with 20 mM KNO_3 or exposed to continuous darkness for 5 d. Red and blue arrows indicate RN and GN. Numbers in the upper right corners indicate the percentage of plants containing GN ($n = 16$–24 for each treatment). Note that all the analyzed control (4 wpi) plants contain only RN. Bars, 2 mm and 500 μm in upper and lower panels, respectively. (b, c) Comparison of heme (b) and BV (c) levels in nodules with different treatments. Heme and BV were quantified by determining the ratio of UPLC peak area to that of standards and were normalized against 4 wpi (control) or 4 wpi + Darkness (GN), respectively. Values are means ± SE ($n = 3$) and were analyzed using Tukey's multiple comparison test. Means denoted by the same letter are not significantly different at $P < 0.05$. (d) Scheme of the enzymatic biosynthetic pathway of BV IXα in higher plants. Heme oxygenase (HO) catalyzes the oxygen-dependent cleavage of Fe-PPIX (iron-protoporphyrin IX or heme) to produce BV with concomitant release of Fe^{2+} and CO (carbon monoxide). ALA, δ-aminolevulinic acid.

nodules compared with MG-20 nodules at both 4 and 8 wpi (Fig. S4c), suggesting that *LjHO2* is unaffected in *ho1-1* and *ho1-2* background. At 4 wpi (mature nodule stage), the mutant plants had RN that were similar to those of WT plants (Fig. 4a). However, SNF, estimated as ARA, was significantly inhibited in RN of *ho1-1* (*c.* 23% reduction compared with RN of WT at 4 wpi; Fig. 4c). At 8 wpi (senescent stage), GN emerged in MG-20 plants, whereas BN (brown nodules) were seen in *ho1* mutants, accounting for *c.* 5% of the total nodule number (Fig. 4b,e). Likewise, the formation of BN was observed in two independent *LORE1* insertional mutants (*ho1-3* and *ho1-4*) in Gifu background at 10 wpi, which were completely devoid of LjHO1 protein (Fig. S5a,b,d,h). Microscopic analysis of nodule sections showed that the brown pigment was particularly abundant in the periphery of the nitrogen-fixing zone (Fig. 4b).

The shoot fresh weight of *ho1-1* and *ho1-2* was reduced by *c.* 18% compared with the WT at 4 or 8 wpi (Fig. 4d). The number of RN in the two mutants also decreased significantly (*c.* 31% at 4 wpi and 21% at 8 wpi; Fig. 4e). The decrease in the number of RN was more pronounced (*c.* 77% at 4 wpi and 59% at 10 wpi) in the *ho1-3* and *ho1-4* mutants in Gifu background (Fig. S5c,f). In this case, a grafting experiment showed that the reduced total nodule number of *ho1-3* plants at 4 wpi was caused by the absence of LjHO1 in the shoot (Fig. S5e).

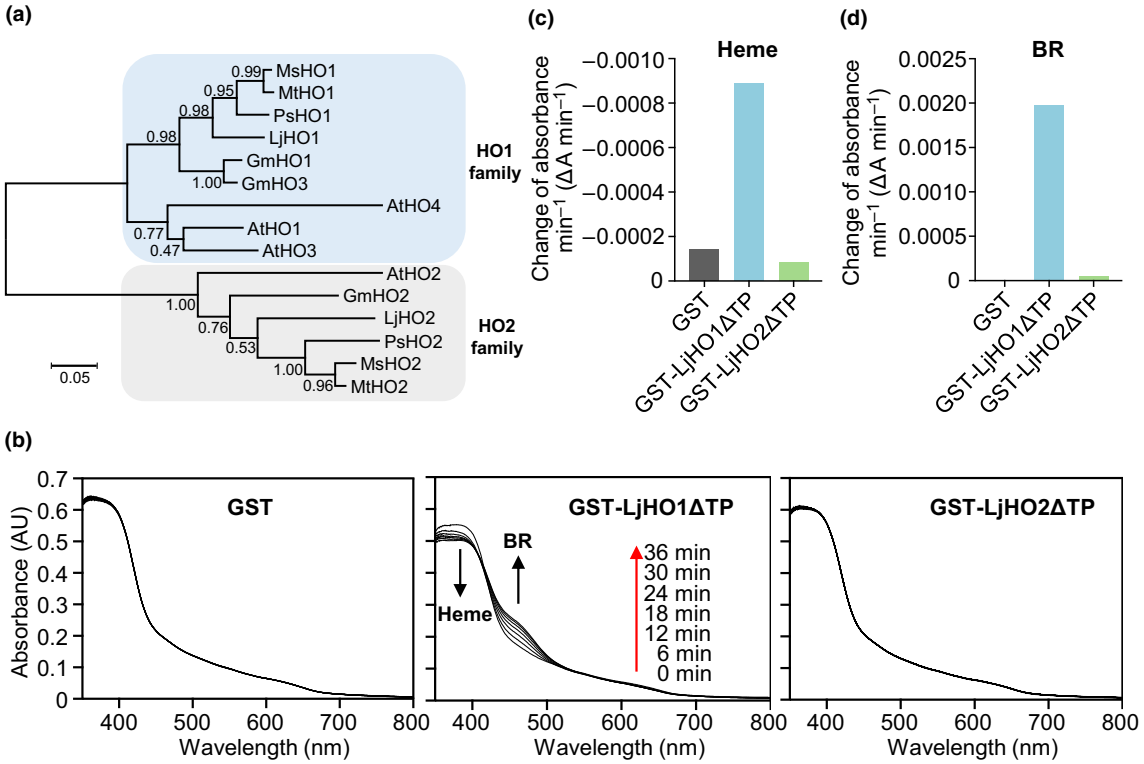

Fig. 2 *LjHO1* encodes a catalytically active heme oxygenase (HO). (a) Phylogenetic tree analysis of two types of HOs (HO1 and HO2 protein families) from *Medicago sativa* (MsHO1 and MsHO2), *Medicago truncatula* (MtHO1 and MtHO2), *Pisum sativum* (PsHO1 and PsHO2), *Lotus japonicus* (LjHO1 and LjHO2), *Glycine max* (GmHO1, GmHO2, and GmHO3), and *Arabidopsis thaliana* (AtHO1, AtHO2, AtHO3, and AtHO4). The maximum likelihood phylogenetic tree was constructed using MEGA7 with 1000 bootstrap replicates. Numbers above branches correspond to Bayesian posterior probabilities. The scale bar indicates the estimated amino acid substitutions per site. (b) HO enzymatic activity assay. Time-course absorbance spectral changes of reaction mixtures containing recombinant GST fusion proteins of LjHO1 or LjHO2 without the corresponding chloroplast transit peptides (GST-LjHO1ΔTP or GST-LjHO2ΔTP) were recorded, using GST as a negative control. Black arrows show absorbance decrease in the substrate heme and increase in the final product bilirubin (BR) generated by a mammalian biliverdin reductase, while the red arrow indicates the time course (0–36 min with 6 min interval) of the assay. (c, d) The rates (change in absorbance per minute, ΔA min^{-1}) of heme consumption (OD at 405 nm) (c) and BR formation (OD at 450 nm) (d) in the HO enzymatic activity assay.

A comparison of RN, GN, and BN formed at the senescent stage reveals that SNF was drastically repressed in the GN of WT and in the BN of *ho1-1* relative to the RN of WT at 8 wpi (Fig. 4c). Immunoblot analysis and heme quantification by HPLC indicated that RN of WT and *ho1-1* at 8 wpi contained similar levels of Lbs and heme, and that both parameters were reduced (*c.* 52–62% for heme and *c.* 14–29% for Lbs) with respect to the corresponding RN at 4 wpi (Fig. 4f,g). By contrast, Lbs were almost completely lost in the GN of WT or totally lost in the BN of *ho1-1* (Fig. 4g). In line with this, the heme content of the WT at 8 wpi was *c.* 86% lower in GN than in RN (Fig. 4f). However, the heme content remained unchanged between the RN and BN in *ho1-1* at 8 wpi (Fig. 4f), in agreement with the essential role of LjHO1 in degrading heme (Fig. 2b–d). Taken together, these data indicate that LjHO1 is required for an efficient SNF in mature nodules and that LjHO1 deficiency leads to heme accumulation and formation of BN at the senescent stage.

The unusual brown color of the *ho1* senescent nodules is reminiscent of the presence of melanin, a type of dark brown or black pigments found in microorganisms, animals, and plants. Melanin is involved in various biological processes such as antioxidant defense, seed camouflage, and pest resistance (Glagoleva *et al.*, 2020). We extracted the brown pigment using a basic aqueous solution and found that the *ho1* BN extract had the most intense color (Fig. S6a). After the addition of acidic reagent, insoluble black precipitation was observed in parallel with loss of brown color, which is a hallmark property of melanin (Fig. S6b; Glagoleva *et al.*, 2020). The solution was decolorized in the presence of strong oxidizing agents, such as potassium permanganate or hydrogen peroxide, whereas exposure to $FeCl_3$ led to the precipitation of a flocculent material (Fig. S6b). These results suggest that the BN of *ho1* may contain melanin-like pigments.

Disruption of rhizobial heme-degrading enzymes does not affect nodule activity in unstressed WT or *ho1-1* nodules but does affect it in stressed WT nodules

Rhizobia encode heme-degrading enzymes (Puri & O'Brian, 2006; Amarelle *et al.*, 2016). To date, four different types of heme-degrading enzymes have been identified in prokaryotic microorganisms, namely, monooxygenases HemO (Ratliff

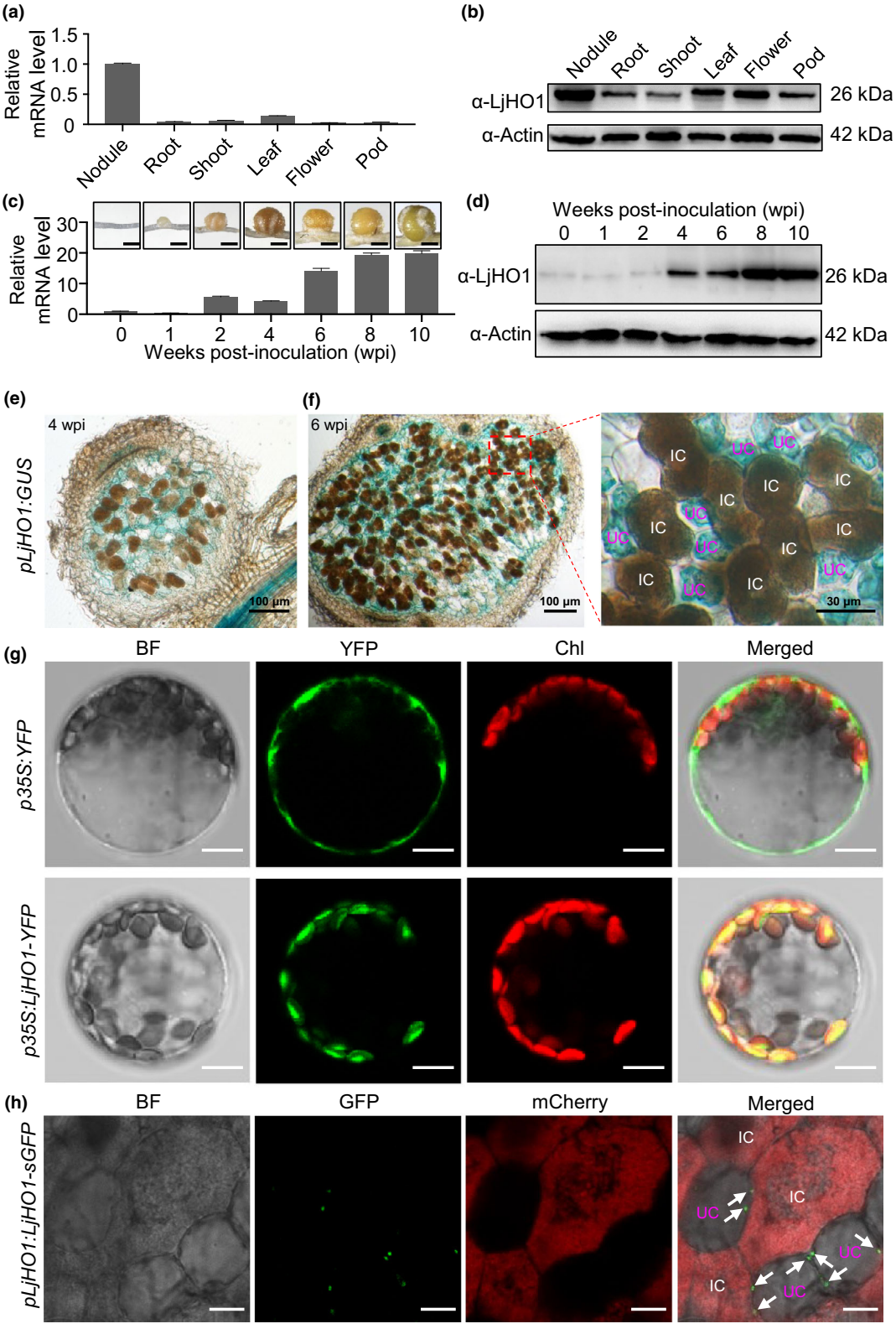

et al., 2001), cytoplasmic heme-binding protein ChuS/PhuS (Suits *et al.*, 2005; Lee *et al.*, 2014), IsdG (Iron-regulated surface determinant) family proteins (Wilks & Ikeda-Saito, 2014), and the radical *S*-adenosyl-methionine (SAM) superfamily ChuW (LaMattina *et al.*, 2016). In *M. loti* MAFF303099, three candidate heme-degrading enzymes were identified by BLAST using query proteins from *Sinorhizobium meliloti* and *E. coli* O157:H7, and these three proteins are named HmuQ (IsdG family

Fig. 3 Expression and subcellular localization of LjHO1. (a–d) qRT-PCR and immunoblot analyses of *LjHO1* transcript and protein abundance in different tissues (a, b) and at different stages of nodule development (c, d). For (a, b), total RNA and protein were obtained from nodules, roots, shoots, and leaves of plants at 4 wk post-inoculation (wpi) and from flowers and pods of plants at 10 wpi. For (c, d), total RNA and protein were obtained from MG-20 uninoculated roots (0 wpi) and nodules from 1 to 10 wpi. In (c), corresponding images of uninoculated roots and nodules were shown above the bar chart. In (a, c), relative mRNA levels were normalized against *LjUBQ1* and the values are means ± SE of three technical replicates. Two biological replicates were analyzed and similar trends of *LjHO1* expression changes were observed. In (b, d), the same amount of protein (*c.* 30 μg) was loaded for each sample. Actin was used as the equal loading control. Bar: (c) 500 μm. (e, f) Expression of *pLjHO1:GUS* in MG-20 nodules at 4 wpi (e) or 6 wpi (f). Images are representative of at least six independently stably transformed plants. Note that the *LjHO1* promoter activity is restricted to uninfected interstitial cells (UC) and is almost absent from infected cells (IC). Bar: (e, f left panel) 100 μm; (f right panel) 30 μm. (g) Localization of LjHO1 in Arabidopsis protoplasts transfected with *p35S:YFP* or *p35S:LjHO1-YFP* vectors. Merged images show overlay of the YFP signal, the chlorophyll autofluorescence (Chl), and the bright field (BF) images. Bar, 10 μm. (h) Subcellular localization of LjHO1 in MG-20 nodules. Hairy root transformed plants expressing *pLjHO1:LjHO1-sGFP* were inoculated with *Mesorhizobium loti* MAFF303099 constitutively expressing mCherry, and nodules at 6 wpi were examined. The merged image shows overlay of the rhizobia (mCherry), the GFP signal, and the bright field (BF) image. White arrows indicate the green punctate signals at the periphery of UC. Bar, 10 μm.

protein), HmuS (cytoplasmic heme-binding protein), and HemW (SAM superfamily protein; Fig. S7a,b).

We employed a homologous recombination-based approach to construct double ($HmuQ^-$ $HmuS^-$) and triple mutants ($HmuQ^-$ $HmuS^-$ $HemW^-$) of these genes, which were confirmed by PCR-based genotyping (Fig. S7c). WT (MG-20) and *ho1-1* plants were inoculated with WT (MAFF303099) or mutant rhizobia, and symbiotic phenotypes, including nodule number, shoot fresh weight, and ARA, were analyzed at 8 wpi. Results showed that the knockout of two or three bacterial genes did not affect the symbiotic phenotype in either WT or *ho1-1* mutant plants (Fig. S7d–f). To further investigate whether these rhizobial mutant-induced nodules are more susceptible to stress treatments, nodulated plants at 4 wpi were supplied with 20 mM KNO_3 or exposed to continuous darkness for 5 d. We found that MG-20 plants inoculated with rhizobia mutants exhibited lower nitrogenase activity after both treatments than the respective plants inoculated with the WT strain. By contrast, rhizobia mutants did not lead to further inhibition of nitrogenase activity under stress conditions in *ho1-1* background (Fig. S7g).

Biliverdin production is blocked in *ho1* mutant nodules

The accumulation of heme in senescent BN of *ho1* prompted us to quantify the heme degradation product BV. As expected, the BV content measured by UPLC-MS/MS was drastically reduced in BN of *ho1-1* as compared with GN of WT (MG-20) at 8 wpi (*c.* 92% reduction; Fig. 5a). The residual amount of BV in *ho1-1* could be due to non-enzymic heme degradation *in vivo* or during sample preparation. To investigate the presence of BV in nodules, we used an engineered BV sensor, iBlueberry, which contains the BV-binding domain of the bacteriophytochrome from *Deinococcus radiodurans* (Yu *et al.*, 2016). Expression of the fusion protein of LjHO1 chloroplast transit peptide and iBlueberry (LjHO1TP-iBlueberry) in hairy-root transgenic plants was driven by the *LjUBQ1* promoter. The fluorescence signal of BV-chromophorylated iBlueberry was clearly detectable in the plastids of UC in WT nodules, whereas no signals were observed in *ho1-1* and *ho1-2* mutant nodules (Fig. 5b). Similar results were obtained for *ho1-3* mutant nodules in Gifu background (Fig. S8). We thus conclude that BV production mainly occurs in the plastids of UC and that the absence of LjHO1 prevents BV production in nodules.

Superoxide production is enhanced in *ho1* nodules

Previous studies have demonstrated the antioxidant roles of HO and BV in plants under stressful environments (Balestrasse *et al.*, 2005, 2008; Zilli *et al.*, 2008). To compare the SNF phenotype under stress conditions, WT (MG-20) and *ho1-1* plants at 4 wpi were treated with 20 mM KNO_3 or exposed to darkness for 5 d. GN emerged on WT roots after nitrate (*c.* 43% of total nodules) or dark (*c.* 60% of total nodules) treatments, whereas BN were found in *ho1-1* (*c.* 39% and 61% of total nodules under the two conditions; Fig. 6a,b). After treatment of plants with nitrate or continuous darkness, the heme contents were reduced by 84–90% in WT nodules but 43–53% in *ho1-1* nodules compared with their corresponding control (untreated) nodules (Fig. 6c). Immunoblots indicated that Lbs were dramatically reduced in both WT and ⁻ upon treatment with nitrate or darkness (Fig. 6d), in line with the changes in transcript abundance of *LjLbs* (Fig. S9). In the WT plants, stress treatments resulted in a *c.* 1.6-fold increase of LjHO1 protein content in GN relative to RN (Fig. 6d). Since Lbs are the dominant hemoproteins in nodules, these results suggest that the remaining higher level of heme in BN of *ho1-1* compared with GN of WT is probably derived from degraded Lbs.

Excess free heme catalyzes the formation of ROS and is highly toxic to plant cells (Tripathy & Oelmuller, 2012). We extracted total heme of nodules with acidic acetone and quantified it by UPLC-MS/MS. In the *ho1-1* mutant, heme was found to accumulate in aging (Fig. 4f) and stressed (Fig. 6c) nodules, and this could trigger oxidative stress. To test this hypothesis, the production of superoxide radicals and H_2O_2 was visualized, respectively, by NBT staining (reduction to blue formazan) and DAB staining (oxidation to brown precipitate) in nodules from plants treated with nitrate or exposed to continuous darkness for 2 d. Two patterns of NBT staining were observed, one in cells throughout the infected zone and the other one, much less frequent, at the periphery of the infected zone; in both cases, preincubation of nodule sections with DPI clearly decreased staining intensity, strongly suggesting that superoxide is being produced at least in

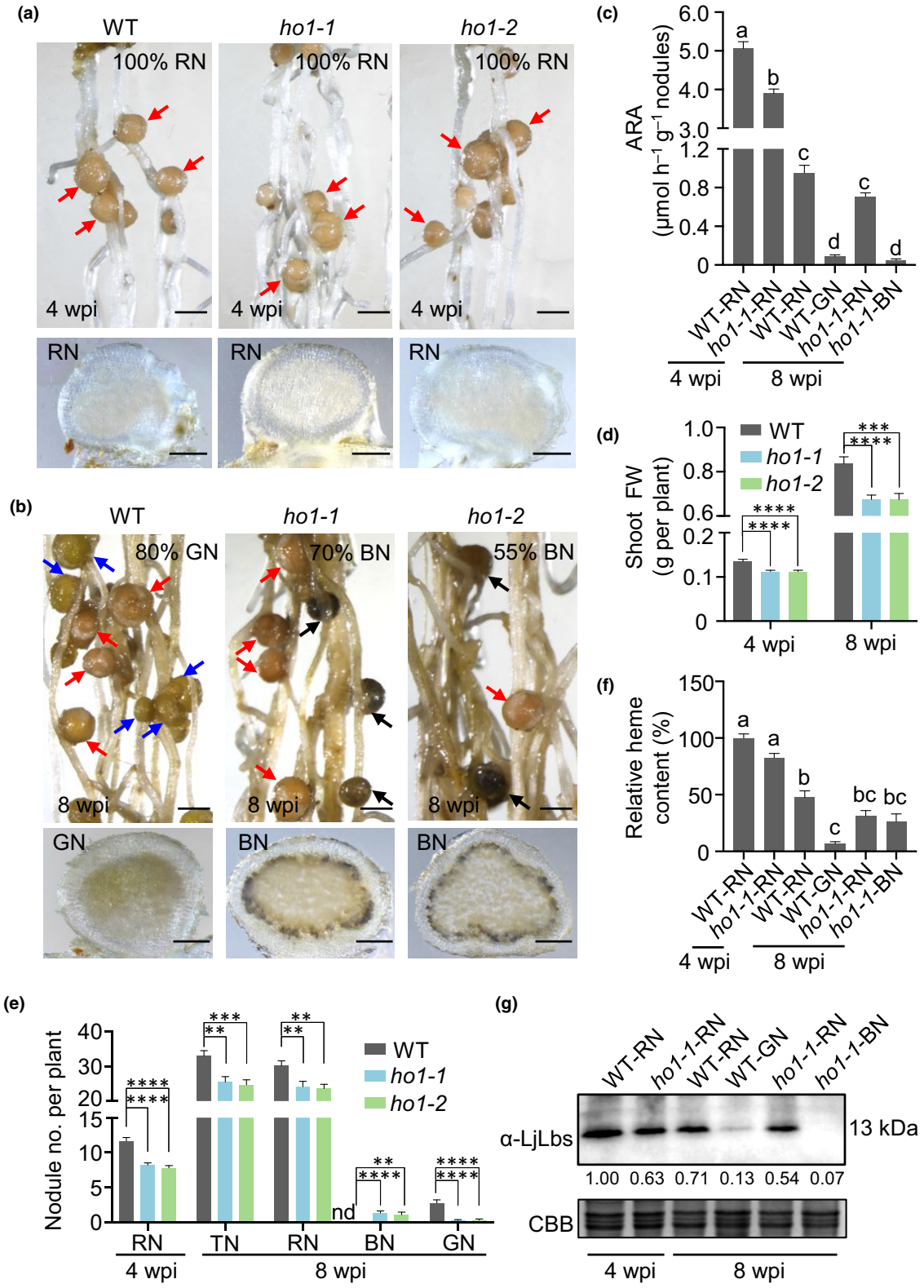

part by NADPH oxidases (Fig. S10a). Notably, RN (control untreated nodules) of *ho1-1* showed more intense staining than RN of WT (Fig. 7a). Because these two types of RN contain similar levels of total heme (Fig. 6c), this discrepancy could be explained by differences of free heme content, which is theoretically maintained low in WT but is probably higher in *ho1*. This explanation is supported by a previous report of enhanced accumulation of free heme in an Arabidopsis *ho1* mutant (Espinas *et al.*, 2012). The same trend was observed for nitrate- and dark-stressed nodules, although in this case *ho1-1*

Fig. 4 Symbiotic phenotypes of *ho1* mutants. (a, b) Root nodules of wild-type (WT) plants (MG-20) and *ho1* mutants (upper panels) and nodule sections (lower panels) at 4 wk post-inoculation (wpi) (a) and 8 wpi (b). Red, blue, and black arrows indicate red nodules (RN), green nodules (GN), and brown nodules (BN). In (a), numbers in the upper right corners indicate the percentage of plants containing RN ($n = 32$–48). Note that all WT and *ho1* mutant plants contained only RN. In (b), numbers in the upper right corners indicate the percentage of plants bearing GN (WT) or BN (*ho1*) out of the total number of analyzed plants ($n = 20$). Bar, 1 mm in the upper panels and 250 μm in the lower panels. (c) Acetylene reduction activity (ARA) of WT (RN or GN) and *ho1-1* (RN or BN) at 4 and 8 wpi. ARA was determined in detached nodulated roots from whole plants at 4 wpi, whereas nodules of the same color (GN, RN, or BN) were stripped from 8 wpi roots and combined for the nitrogenase activity assay. Data are means ± SE of three or four biological replicates, each containing nodules from five or six plants. (d) Shoot fresh weight (FW) of nodulated plants at 4 and 8 wpi. Data are means ± SE ($n \geq 32$, 4 wpi; $n = 24$, 8 wpi). (e) Number of RN, GN, and BN formed on WT, *ho1-1*, and *ho1-2* mutants at 4 and 8 wpi. Data are means ± SE ($n \geq 32$, 4 wpi; $n = 20$, 8 wpi). nd, non-detectable; TN, total nodules. (f) Comparison of heme content in WT and *ho1-1* nodules. Heme levels were normalized against WT-RN at 4 wpi. Data are means ± SE of three or four biological replicates. Each replicate contained nodules from six plants. (g) Immunoblot analysis of leghemoglobins (LjLbs) in WT and *ho1-1* nodules at 4 and 8 wpi. Coomassie Brilliant Blue (CBB) staining was used as the loading control. ImageJ was used to quantify relative band intensities in anti-Lb immunoblots. For (c, f), statistical analysis was performed by Tukey's multiple comparison test. Means denoted by the same letter are not significantly different at $P < 0.05$. For (d, e), Student's *t*-test was used to compare *ho1-1* or *ho1-2* mutants with WT. **, $P < 0.01$; ***, $P < 0.001$; ****, $P < 0.0001$.

nodules were only slightly more stained than the corresponding WT nodules (Fig. 7a).

Unlike superoxide production, we found only little differences in H_2O_2 production between WT and *ho1-1* both in control and in nitrate/dark-stressed nodules (Fig. 7b). Preincubation of nodule sections with scavengers confirms that DAB oxidation is due to H_2O_2 (Fig. S10b). These data suggest that mis-accumulated free heme leads to enhanced superoxide production without major impact on the H_2O_2 content of nodules. Taken together, these results indicate that nitrate and dark stress accelerate Lb degradation in nodules and that LjHO1 plays a protective role by mitigating the oxidative stress triggered by free heme.

Discussion

Nodule cells synthesize high amounts of heme that are required for diverse processes indispensable for SNF, especially as a component of Lbs and cytochromes. However, free (protein unbound) heme is cytotoxic and therefore its concentration requires strict homeostasis. Here, we report the novel finding that heme is catabolized by HO in the plastids of UC and unequivocally identify BV as the enzymatic product in nodules. The current view is that the UC are involved in the metabolism of sucrose to malic acid and in the production of ureides in determinate nodules (White *et al.*, 2007). An exception is *L. japonicus* because this legume transports asparagine instead of ureides to the shoot as the main nitrogen compound derived from SNF (Tajima *et al.*, 2000). Notably, in the *lb123* mutant nodules that are devoid of Lbs, the expression of *LjHO1* is enhanced with respect to WT nodules, probably as a result of the oxidative stress ensued in the mutant nodules (Wang *et al.*, 2019). Here we show that the *ho1* mutant nodules also experience oxidative stress, as evidenced by an exacerbated production of superoxide radicals (Fig. 7a). Thus, our finding of HO specifically in the plastids of UC uncovers a new role of these cells in protecting and supporting SNF.

The deficiency of LjHO1 caused the formation of BN instead of GN during nodule senescence, in agreement with the blockage of BV production in the *ho1* mutant nodules. At the initial stage of nodule maturation, many plant genes of the heme biosynthetic pathway are upregulated to keep pace with the increased level of Lbs (Sangwan & O'Brian, 1999; Wang *et al.*, 2019, 2022). Expression of *LjHO1* is high in mature nodules and further enhanced in aging nodules (Fig. 3c,d). Free heme is released from the turnover of Lbs (Bisseling *et al.*, 1980), which may stimulate the expression of *LjHO1* in nodule cells.

An early immunogold localization study with soybean nodules reported that Lb is present in the cytoplasm and nuclei of UC at amounts that are *c.* 25% those found in IC (VandenBosch & Newcomb, 1988). Using immunogold labeling, we have also detected Lb in the UC of *L. japonicus* nodules (Fig. S11). Regardless of whether the protein found in the UC of both legume nodules is apo-Lb or holo-Lb, these data strongly suggest that Lb is synthesized within the UC, albeit at lower amounts than in IC. The heme synthesized in the nodule bacteroids and plastids (Sangwan & O'Brian, 1991, 1999; Santana *et al.*, 1998) may assemble with apo-Lb in the UC, thereby producing functional Lb. An alternative explanation is that Lb itself passes from IC to UC through the plasmodesmata, but this is unlikely due to constraints of protein size (VandenBosch & Newcomb, 1988). Consequently, the most plausible explanation for our findings is that the heme of Lb produced in IC and transported to UC, as well as the heme probably generated in the plastids of UC, are degraded to BV by HO during senescence and stress conditions. For simplicity, this is shown in a model taking into account only Lb produced in IC (Fig. 8). In any case, the potential functions of Lb in UC such as providing O_2 to mitochondria, as well as Lb catabolism, deserve further investigation.

In senescing nodules, the degradation of Lb and the destruction of IC result in additional increases of intracellular free heme, which may, in turn, induce LjHO1 to degrade the excess of free heme and keep it at a very low steady-state level. Hence, the induction of LjHO1 is tightly linked to the demand for detoxification of free heme in nodules. This conclusion is reinforced by previous observations that HO is upregulated in response to diverse types of stress in soybean roots and nodules (Balestrasse *et al.*, 2005, 2008; Zilli *et al.*, 2008) and in alfalfa (Baudouin *et al.*, 2004). Moreover, the production of BV detected in our study also supports a protective role of HO because BV displays

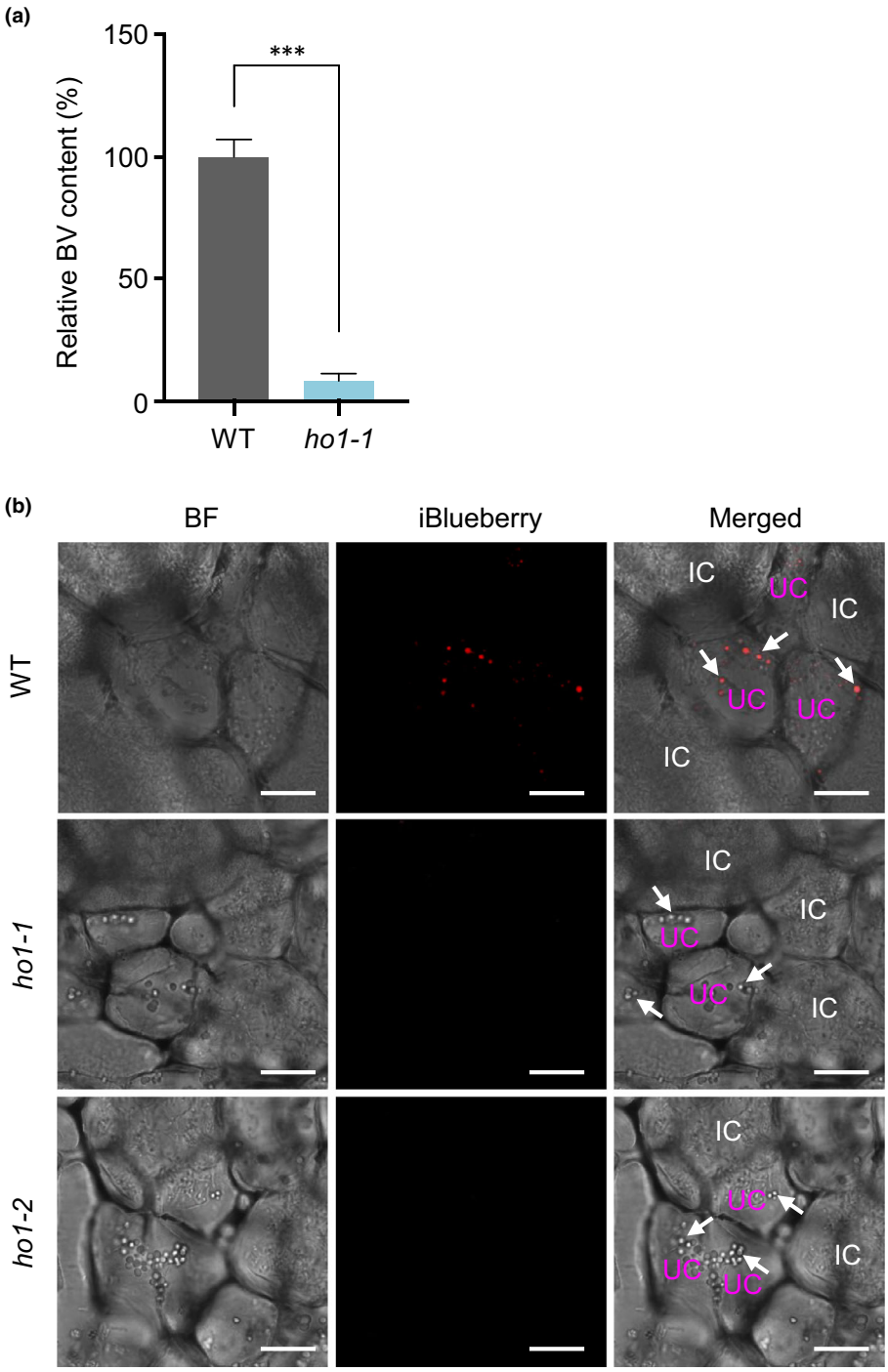

Fig. 5 LjHO1 is required for biliverdin (BV) production in the plastids of uninfected interstitial cells (UC) of nodules. (a) BV content in wild-type (WT; MG-20) and *ho1-1* nodules at 8 wk post-inoculation (wpi). Quantification of BV was performed by determining the ratio of its UPLC peak area to that of BV standard. Data are means ± SE of three biological replicates. Each replicate contained nodules from six plants. Statistical analysis was performed using Student's *t*-test. ***, $P < 0.001$. (b) Detection of BV production by expression of the plastid-targeted BV sensor iBlueberry. Nodules of hairy root transformed plants at 6 wpi were sectioned and analyzed by super-resolution fluorescence microscopy. BV-chromophorylated iBlueberry protein was excited at 644 nm and the fluorescence signal was acquired at 655–700 nm, with the peak wavelength at 667 nm. Note that the iBlueberry fluorescence was clearly visible in the plastids of UC of WT nodules (white arrows), but absent from *ho1* nodules. BF, bright field; IC, infected cells. Bars, 10 μm.

antioxidant properties (Mahawar & Shekhawat, 2018). The identification of nitrated heme, a green derivative of Lbs, suggests that highly oxidizing and nitrating species are produced in senescent nodules (Navascués *et al.*, 2012). This finding is consistent with the upregulation of LjHO1 in senescent nodules, which results in the degradation of cytotoxic free heme and production of the antioxidant, BV.

Heme is actively synthesized in the IC of nodules, whereas *LjHO1* is predominantly expressed in UC (Fig. 3e,f,h). The spatial separation of heme synthesis and its degradation confer several advantages. First, heme degradation by LjHO1 requires O_2 (Shekhawat & Verma, 2010), the concentration of which is very low in IC (*c.* 3–28 nM) due to the Lb buffering capacity (Becana & Klucas, 1992). The localization of HO in UC, with a high availability of O_2, is therefore more conducive for an efficient decomposition of heme. Second, the spatial separation of Lbs and CO, a byproduct of heme degradation, may avoid the poisoning of Lbs by CO because Lbs have a much higher affinity for CO than for O_2 (Martin *et al.*, 1990). Furthermore, heme is an iron source in nodules and may be degraded by HO during

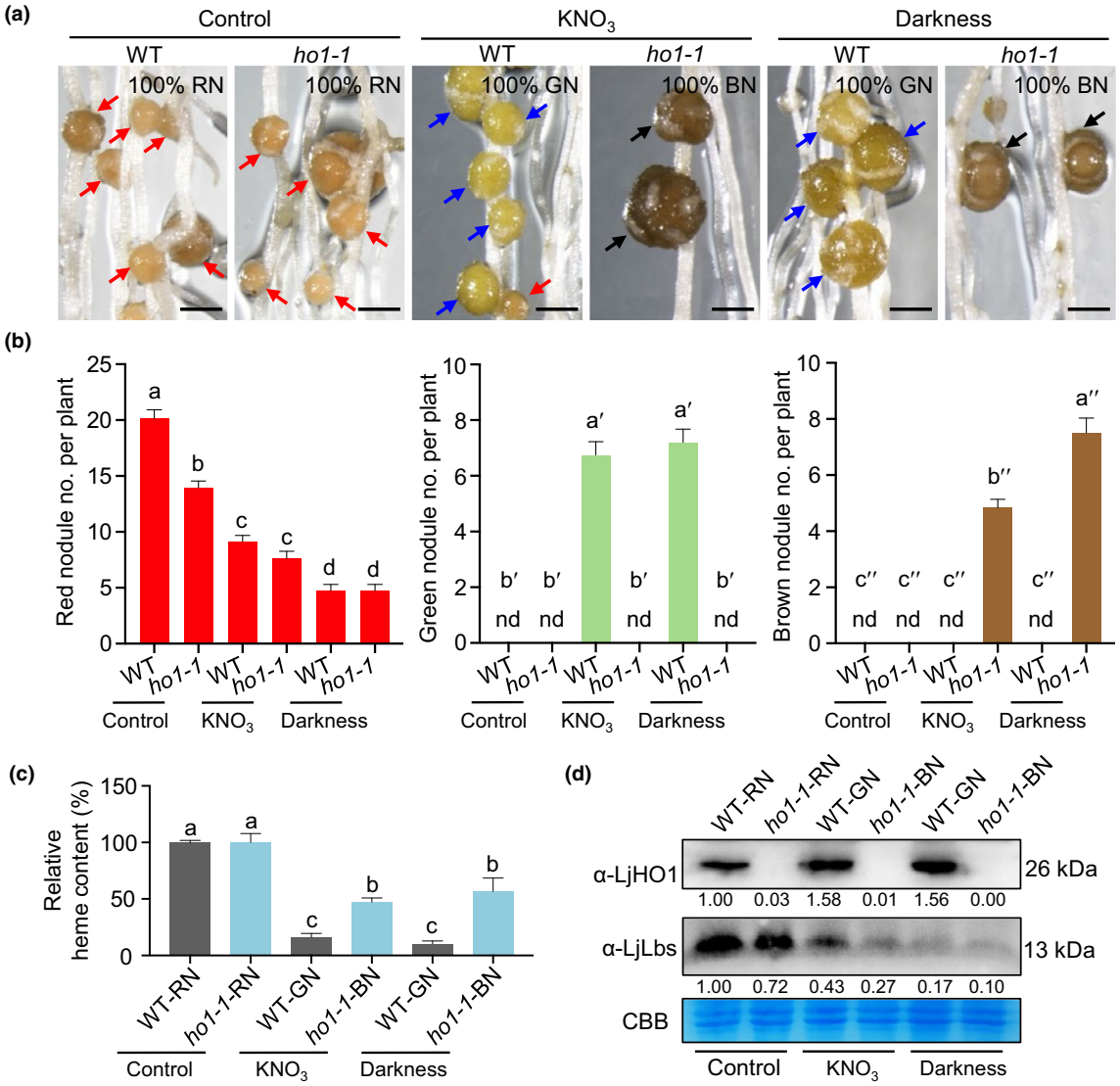

Fig. 6 Formation of green nodules in wild-type (WT) plants and brown nodules in *ho1* plants. (a) Morphology of WT (MG-20) and *ho1-1* nodules at 4 wk post-inoculation (wpi) after treatment of plants with 20 mM KNO_3 or continuous darkness for 5 d. Controls were WT and *ho1-1* plants at 4 wpi growing for another 5 d without stress treatment. Red, blue, and black arrows indicate red nodules (RN), green nodules (GN), and brown nodules (BN). Bar, 2 mm. For controls, numbers in the upper right corners indicate the percentage of plants containing RN ($n = 24$). For KNO_3 or darkness treatments, numbers in the upper right corners indicate the percentage of plants containing GN (WT) or BN (*ho1*) with respect to the total number of examined plants ($n = 24$). (b) Number of RN, GN, and BN per plant under the conditions specified in (a). nd, non-detectable. Data are means ± SE ($n = 24$). (c) Comparison of relative heme contents of WT and *ho1-1* nodules. Heme content values were normalized against WT-RN (Control). Data are means ± SE of three biological replicates, each containing nodules from eight plants. (d) Immunoblot analysis of LjHO1 and LjLbs. Coomassie Brilliant Blue (CBB) staining was used as the equal loading control. ImageJ was used to quantify relative band intensities in anti-HO1 and anti-Lb immunoblots. In (b, c), statistical analysis was performed by Tukey's multiple comparison test. Means denoted by the same letter are not significantly different at $P < 0.05$.

nodule senescence to recycle iron. A previous study showed that *c.* 40–59% of the iron content in soybean seeds might originate from senescing nodules (Burton *et al.*, 1998). The accumulation of ferritin in the UC and cortical cells of nodules also supports the potential role of these cells in iron reutilization and protection against oxidative stress (Lucas *et al.*, 1998; Matamoros *et al.*, 1999). In humans, heme is massively produced in red blood cells, whereas its degradation occurs in macrophages and is mediated by HO; in fact, macrophages are responsible for the degradation of toxic free heme, the recycling of iron, and the production of antioxidant and anti-inflammatory compounds, BV, and CO (Vijayan *et al.*, 2018). Hence, the spatiotemporal separation of heme biosynthesis and heme degradation in different nodule cells is a model of labor division among functionally distinct cell types.

During developmental nodule senescence, *c.* 5% nodules of *ho1* mutants turned brown or dark brown (Figs 4b,e, S5d,h). BN has been identified in *L. japonicus apn1* mutant with the disruption of *ASPARTIC PEPTIDASE NODULE-INDUCED 1*. However, the mechanism of BN formation in *apn1* mutant is

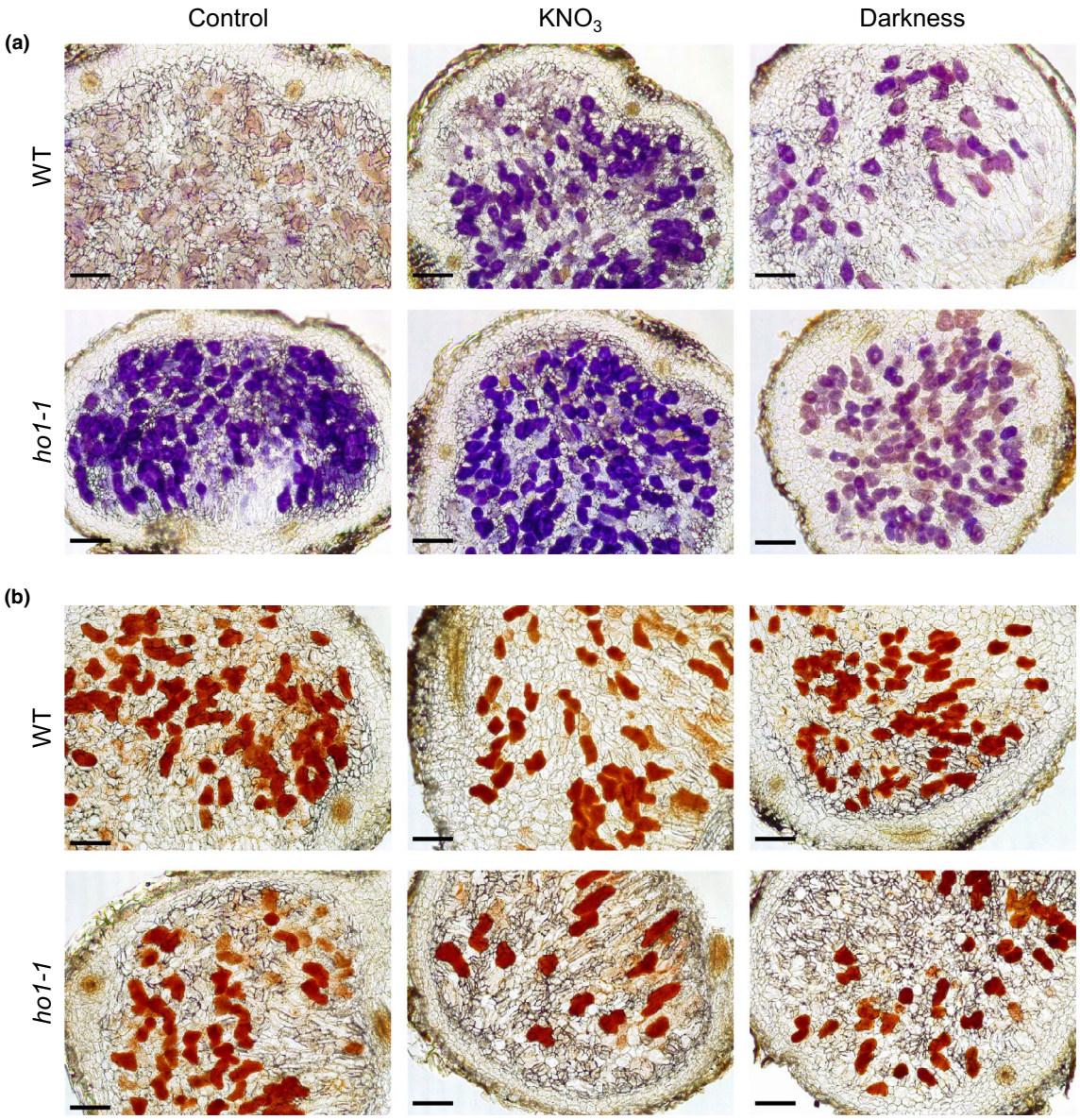

Fig. 7 Production of superoxide and H_2O_2 in nodules of *ho1-1* mutant plants. Nitroblue tetrazolium and diaminobenzidine staining were used for the detection of superoxide (a) and H_2O_2 (b), respectively. Wild-type (WT) and *ho1-1* plants at 5 wk post-inoculation were treated with 20 mM KNO_3 or exposed to continuous darkness for 2 d. Untreated controls were run in parallel. In (a, b), a total of 16 nodule sections (eight nodules, each with two sections) were analyzed for each treatment and representative images are shown. Bars: (a, b) 150 μm.

unknown (Yamaya-Ito *et al.*, 2017; Shimoda *et al.*, 2020). In addition, the dark BN of the *ho1* mutant contain melanin-like pigments (Fig. S6), unlike the BN of *M. truncatula* that accumulate phenolic compounds (Bourcy *et al.*, 2013; Berrabah *et al.*, 2014; C. Wang *et al.*, 2016; Pislariu *et al.*, 2019). Melanin is produced by the oxidation and polymerization of phenolic compounds catalyzed by plastid-located polyphenol oxidases in the presence of O_2 (Glagoleva *et al.*, 2020). In *ho1* mutant nodules, brown compounds are mainly concentrated at the periphery of the nitrogen-fixing zone adjacent to the cortical cells (Fig. 4b). Compared with the central zone, this area is more likely to be exposed to external O_2 and oxidative stress, which may contribute to the accumulation of melanin-like pigments.

In conclusion, this study reveals that heme catabolic pathway is located at a very specific location within the nodules and uncovers a novel role of plastids of UC in protecting SNF. Our results suggest an intercellular transport of Lb heme from IC to UC. In these cells, heme is translocated to the plastids and degraded to BV, as proven by using *ho1* mutants. Future investigation of these transporting mechanisms should provide deeper insights into SNF functioning in legume nodules.

Acknowledgements

We thank three anonymous reviewers for helpful comments on the manuscript. We are grateful to Dr Euan K. James (The James

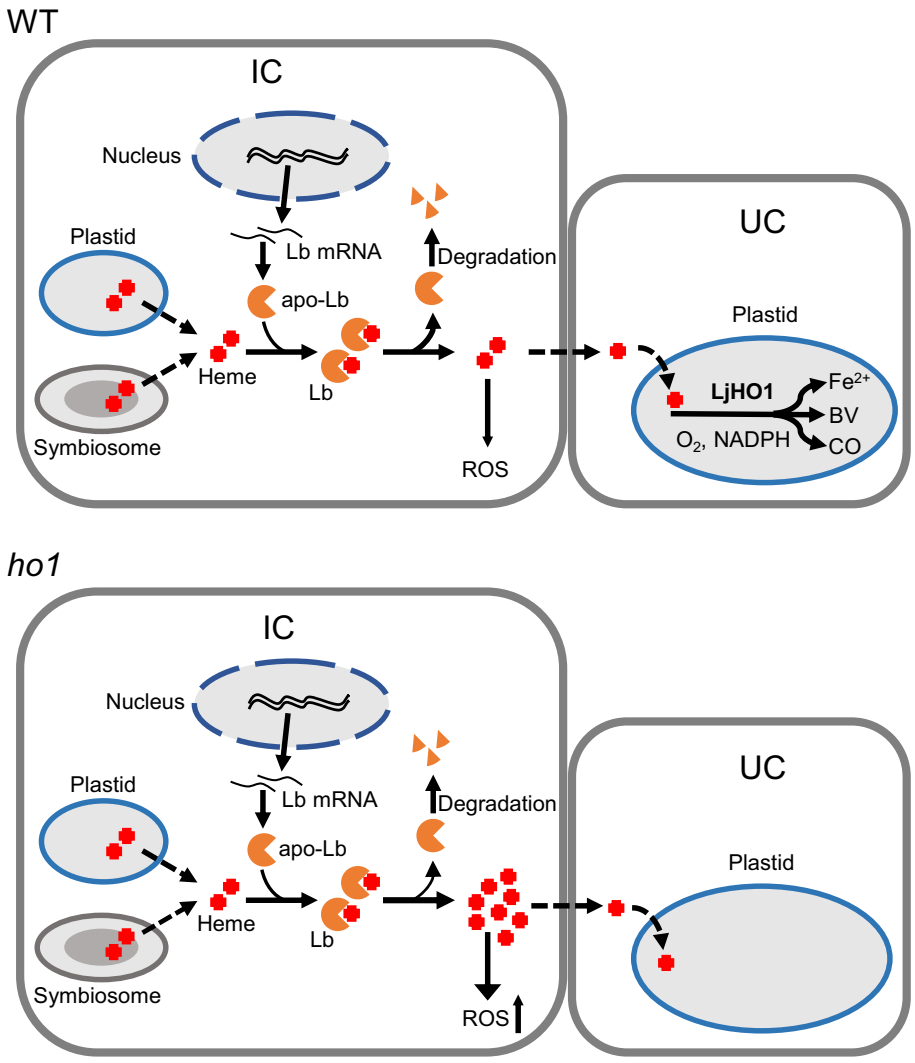

Fig. 8 Model for the role of HO1 in maintaining an efficient symbiotic nitrogen fixation in nodules. In infected cells (IC), heme derived from the tetrapyrrole biosynthetic pathway from plastids or bacteroids is exported by unknown routes to the cytosol to assemble with apoleghemoglobin (apo-Lb) into functional Lb. In mature nodules and during naturally aging or stress-induced nodule senescence, heme is released from Lbs and transported to the plastids of uninfected interstitial cells (UC), where heme is degraded by LjHO1 with the release of biliverdin (BV), ferrous iron (Fe^{2+}), and carbon monoxide (CO). Oxygen and NADPH are required for the HO1-catalyzed reaction. In the *ho1* mutant, the level of free heme is enhanced, leading to accumulation of reactive oxygen species (ROS) and ensuing oxidative stress. Note that Lb may be present also in UC (Supporting Information Fig. S11) and provide heme as substrate for LjHO1. For simplicity, the current model takes into account only Lb produced in IC. Experimentally proven and hypothetical paths are indicated by solid and dashed lines, respectively.

Hutton Institute, UK) for help with Fig. S11, Prof. Xiaokun Shu (University of California San Francisco, USA) for providing plasmids encoding iBlueberry, and Dr Linlin Zhong (Huazhong Agricultural University, China) for help with the UPLC-MS/MS. This work was supported by the Ministry of Science and Technology of the People's Republic of China (2021YFA0910800), National Natural Science Foundation of China (31870220), the Foundation of Hubei Hongshan Laboratory (2022hszd014), HZAU-AGIS Cooperation Fund (SZYJY2022005), and MCIN/AEI/10.13039/501100011033 of Spain (grant PID2020-113985GB-I00).

Competing interests

None declared.

Author contributions

Yu Zhou, LW, MB, and DD designed the research. Yu Zhou, MCR, CP-R, Yumiao Zhou, YQ, TT, and QF performed the experiments. Yu Zhou, LW, WZ, MCR, CP-R, MB, and DD analyzed the data. Yu Zhou, LW, WZ, MB, and DD wrote and revised the manuscript.

ORCID

Manuel Becana https://orcid.org/0000-0002-1083-0804
Deqiang Duanmu https://orcid.org/0000-0002-9365-362X
Carmen Pérez-Rontomé https://orcid.org/0000-0002-9772-3170
Maria Carmen Rubio https://orcid.org/0000-0002-9378-7775
Longlong Wang https://orcid.org/0000-0003-0537-2711
Yu Zhou https://orcid.org/0000-0001-7743-0517

Data availability

The data that support the findings of this study are available in the article and its Supporting Information. Accession numbers of genes described in this study are as follows: *LjHO1*,

Lj1g3v0672150; *LjHO2*, Lj5g0008202; *LjLb1*, Lj5g3v0035290.2; *LjLb2*, Lj5g3v0035290.1; *LjLb3*, Lj5g3v0465970; *LjUBQ1*, Lj5g3v2060710; *AtHO1*, AT2G26670; *AtHO2*, AT2G26550; *AtHO3*, AT1G69720; *AtHO4*, AT1G58300; *GmHO1*, Glyma.04g147700; *GmHO2*, Glyma.14g081000; *GmHO3*, Glyma.06g221900; *MtHO1*, Medtr8g019320; *MtHO2*, Medtr1g019970; *MsHO1*, ADK12637; *MsHO2*, ADV15621; *PsHO1*, XP_050887870; *PsHO2*, XP_050887605; *HmuQ*, WP_010909951; *HmuS*, WP_010909945; *HemW*, WP_010912579.

References

Adir N, Bar-Zvi S, Harris D. 2020. The amazing phycobilisome. *Biochimica et Biophysica Acta Bioenergetics* **1861**: 148047.

Amarelle V, Rosconi F, Lázaro-Martínez JM, Buldain G, Noya F, O'Brian MR, Fabiano E. 2016. HmuS and HmuQ of *Ensifer/Sinorhizobium meliloti* degrade heme *in vitro* and participate in heme metabolism *in vivo*. *Biometals* **29**: 333–347.

Anzaldi LL, Skaar EP. 2010. Overcoming the heme paradox: heme toxicity and tolerance in bacterial pathogens. *Infection and Immunity* **78**: 4977–4989.

Balestrasse KB, Noriega GO, Batlle A, Tomaro ML. 2005. Involvement of heme oxygenase as antioxidant defense in soybean nodules. *Free Radical Research* **39**: 145–151.

Balestrasse KB, Yannarelli GG, Noriega GO, Batlle A, Tomaro ML. 2008. Heme oxygenase and catalase gene expression in nodules and roots of soybean plants subjected to cadmium stress. *Biometals* **21**: 433–441.

Baudouin E, Frendo P, Le Gieuher M, Puppo A. 2004. A *Medicago sativa* haem oxygenase gene is preferentially expressed in root nodules. *Journal of Experimental Botany* **55**: 43–47.

Baulcombe D, Verma DP. 1978. Preparation of a complementary DNA for leghaemoglobin and direct demonstration that leghaemoglobin is encoded by the soybean genome. *Nucleic Acids Research* **5**: 4141–4155.

Becana M, Klucas RV. 1992. Oxidation and reduction of leghemoglobin in root nodules of leguminous plants. *Plant Physiology* **98**: 1217–1221.

Berrabah F, Bourcy M, Eschstruth A, Cayrel A, Guefrachi I, Mergaert P, Wen J, Jean V, Mysore KS, Gourion B *et al.* 2014. A nonRD receptor-like kinase prevents nodule early senescence and defense-like reactions during symbiosis. *New Phytologist* **203**: 1305–1314.

Bisseling T, van Straten J, Houwaard F. 1980. Turnover of nitrogenase and leghemoglobin in root nodules of *Pisum sativum*. *Biochimica et Biophysica Acta* **610**: 360–370.

Bourcy M, Brocard L, Pislariu CI, Cosson V, Mergaert P, Tadege M, Mysore KS, Udvardi MK, Gourion B, Ratet P. 2013. *Medicago truncatula* DNF2 is a PI-PLC-XD-containing protein required for bacteroid persistence and prevention of nodule early senescence and defense-like reactions. *New Phytologist* **197**: 1250–1261.

Broughton WJ, Dilworth MJ. 1971. Control of leghaemoglobin synthesis in snake beans. *Biochemical Journal* **125**: 1075–1080.

Burton JW, Harlow C, Theil EC. 1998. Evidence for reutilization of nodule iron in soybean seed development. *Journal of Plant Nutrition* **21**: 913–927.

Chiabrando D, Vinchi F, Fiorito V. 2014. Heme in pathophysiology: a matter of scavenging, metabolism and trafficking across cell membranes. *Frontiers in Pharmacology* **5**: 61.

Dhanushkodi R, Matthew C, McManus MT, Dijkwel PP. 2018. Drought-induced senescence of *Medicago truncatula* nodules involves serpin and ferritin to control proteolytic activity and iron levels. *New Phytologist* **220**: 196–208.

Du M, Gao Z, Li X, Liao H. 2020. Excess nitrate induces nodule greening and reduces transcript and protein expression levels of soybean leghaemoglobins. *Annals of Botany* **126**: 61–72.

Duanmu D, Casero D, Dent RM, Gallaher S, Yang W, Rockwell NC, Martin SS, Pellegrini M, Niyogi KK, Merchant SS *et al.* 2013. Retrograde bilin signaling enables *Chlamydomonas* greening and phototrophic survival. *Proceedings of the National Academy of Sciences, USA* **110**: 3621–3626.

Dunand C, Crèvecoeur M, Penel C. 2007. Distribution of superoxide and hydrogen peroxide in Arabidopsis root and their influence on root development: possible interaction with peroxidases. *New Phytologist* **174**: 332–341.

Espinas NA, Kobayashi K, Takahashi S, Mochizuki N, Masuda T. 2012. Evaluation of unbound free heme in plant cells by differential acetone extraction. *Plant & Cell Physiology* **53**: 1344–1354.

Gisk B, Yasui Y, Kohchi T, Frankenberg-Dinkel N. 2010. Characterization of the haem oxygenase protein family in *Arabidopsis thaliana* reveals a diversity of functions. *Biochemical Journal* **425**: 425–434.

Glagoleva AY, Shoeva OY, Khlestkina EK. 2020. Melanin pigment in plants: current knowledge and future perspectives. *Frontiers in Plant Science* **11**: 770.

Herrada G, Puppo A, Moreau S, Day DA, Rigaud J. 1993. How is leghemoglobin involved in peribacteroid membrane degradation during nodule senescence? *FEBS Letters* **326**: 33–38.

Hunt S, Layzell DB. 1993. Gas exchange of legume nodules and the regulation of nitrogenase activity. *Annual Review of Plant Biology* **44**: 483–511.

Jiang S, Jardinaud MF, Gao J, Pecrix Y, Wen J, Mysore K, Xu P, Sanchez-Canizares C, Ruan Y, Li Q *et al.* 2021. NIN-like protein transcription factors regulate leghemoglobin genes in legume nodules. *Science* **374**: 625–628.

Kaneko T, Nakamura Y, Sato S, Asamizu E, Kato T, Sasamoto S, Watanabe A, Idesawa K, Ishikawa A, Kawashima K *et al.* 2000. Complete genome structure of the nitrogen-fixing symbiotic bacterium *Mesorhizobium loti*. *DNA Research* **7**: 331–338.

Korolnek T, Hamza I. 2015. Macrophages and iron trafficking at the birth and death of red cells. *Blood* **125**: 2893–2897.

LaMattina JW, Nix DB, Lanzilotta WN. 2016. Radical new paradigm for heme degradation in *Escherichia coli* O157:H7. *Proceedings of the National Academy of Sciences, USA* **113**: 12138–12143.

Larrainzar E, Villar I, Rubio MC, Pérez-Rontomé C, Huertas R, Sato S, Mun JH, Becana M. 2020. Hemoglobins in the legume–*Rhizobium* symbiosis. *New Phytologist* **228**: 472–484.

Lee MJY, Schep D, McLaughlin B, Kaufmann M, Jia Z. 2014. Structural analysis and identification of PhuS as a heme-degrading enzyme from *Pseudomonas aeruginosa*. *Journal of Molecular Biology* **426**: 1936–1946.

Legris M, Ince YC, Fankhauser C. 2019. Molecular mechanisms underlying phytochrome-controlled morphogenesis in plants. *Nature Communications* **10**: 5219.

Lehtovaara P, Perttilä U. 1978. Bile-pigment formation from different leghaemoglobins. Methine-bridge specificity of coupled oxidation. *Biochemical Journal* **176**: 359–364.

Lei Y, Lu L, Liu HY, Li S, Xing F, Chen LL. 2014. CRISPR-P: a web tool for synthetic single-guide RNA design of CRISPR-system in plants. *Molecular Plant* **8**: 1494–1496.

Lindström K, Mousavi SA. 2020. Effectiveness of nitrogen fixation in rhizobia. *Microbial Biotechnology* **13**: 1314–1335.

Lucas MM, Van de Sype G, Hérouart D, Hernández MJ, Puppo A, de Felipe MR. 1998. Immunolocalization of ferritin in determinate and indeterminate legume root nodules. *Protoplasma* **204**: 61–70.

Mahawar L, Shekhawat GS. 2018. Haem oxygenase: a functionally diverse enzyme of photosynthetic organisms and its role in phytochrome chromophore biosynthesis, cellular signalling and defence mechanisms. *Plant, Cell & Environment* **41**: 483–500.

Martin KD, Saari L, Guang-Xin W, Wang T, Parkhurst LJ, Klucas RV. 1990. Kinetics and thermodynamics of oxygen, CO, and azide binding by the subcomponents of soybean leghemoglobin. *Journal of Biological Chemistry* **265**: 19588–19593.

Matamoros MA, Baird LM, Escuredo PR, Dalton DA, Minchin FR, Iturbe-Ormaetxe I, Rubio MC, Moran JF, Gordon AJ, Becana M. 1999. Stress-induced legume root nodule senescence. Physiological, biochemical, and structural alterations. *Plant Physiology* **121**: 97–112.

Muramoto T, Kohchi T, Yokota A, Hwang I, Goodman HM. 1999. The Arabidopsis photomorphogenic mutant *hy1* is deficient in phytochrome chromophore biosynthesis as a result of a mutation in a plastid heme oxygenase. *Plant Cell* **11**: 335–348.

Navascués J, Pérez-Rontomé C, Gay M, Marcos M, Yang F, Walker FA, Desbois A, Abián J, Becana M. 2012. Leghemoglobin green derivatives with

nitrated hemes evidence production of highly reactive nitrogen species during aging of legume nodules. *Proceedings of the National Academy of Sciences, USA* **109**: 2660–2665.

Ott T, Sullivan J, James EK, Flemetakis E, Günther C, Gibon Y, Ronson C, Udvardi M. 2009. Absence of symbiotic leghemoglobins alters bacteroid and plant cell differentiation during development of *Lotus japonicus* root nodules. *Molecular Plant–Microbe Interactions* **22**: 800–808.

Ott T, van Dongen JT, Günther C, Krusell L, Desbrosses G, Vigeolas H, Bock V, Czechowski T, Geigenberger P, Udvardi MK. 2005. Symbiotic leghemoglobins are crucial for nitrogen fixation in legume root nodules but not for general plant growth and development. *Current Biology* **15**: 531–535.

Pislariu CI, Sinharoy S, Torres-Jerez I, Nakashima J, Blancaflor EB, Udvardi MK. 2019. The nodule-specific PLAT domain protein NPD1 is required for nitrogen-fixing symbiosis. *Plant Physiology* **180**: 1480–1497.

Puppo A, Groten K, Bastian F, Carzaniga R, Soussi M, Lucas MM, de Felipe MR, Harrison J, Vanacker H, Foyer CH. 2005. Legume nodule senescence: roles for redox and hormone signalling in the orchestration of the natural aging process. *New Phytologist* **165**: 683–701.

Puri S, O'Brian MR. 2006. The *hmuQ* and *hmuD* genes from *Bradyrhizobium japonicum* encode heme-degrading enzymes. *Journal of Bacteriology* **188**: 6476–6482.

Ratliff M, Zhu W, Deshmukh R, Wilks A, Stojiljkovic I. 2001. Homologues of neisserial heme oxygenase in gram-negative bacteria: degradation of heme by the product of the *pigA* gene of *Pseudomonas aeruginosa*. *Journal of Bacteriology* **183**: 6394–6403.

Roy S, Liu W, Nandety RS, Crook A, Mysore KS, Pislariu CL, Frugoli J, Dickstein R, Udvardi MK. 2020. Celebrating 20 years of genetic discoveries in legume nodulation and symbiotic nitrogen fixation. *Plant Cell* **32**: 15–41.

Rubio MC, Becana M, Kanematsu S, Ushimaru T, James EK. 2009. Immunolocalization of antioxidant enzymes in high-pressure frozen root and stem nodules of *Sesbania rostrata*. *New Phytologist* **183**: 395–407.

Sandalio LM, Rodríguez-Serrano M, Romero-Puertas MC, del Río LA. 2008. Imaging of reactive oxygen species and nitric oxide *in vivo* in plant tissues. *Methods in Enzymology* **440**: 397–409.

Sangwan I, O'Brian MR. 1991. Evidence for an inter-organismic heme biosynthetic pathway in symbiotic soybean root nodules. *Science* **251**: 1220–1222.

Sangwan I, O'Brian MR. 1999. Expression of a soybean gene encoding the tetrapyrrole-synthesis enzyme glutamyl-tRNA reductase in symbiotic root nodules. *Plant Physiology* **119**: 593–598.

Santana MA, Pihakaski-Maunsbach K, Sandal N, Marcker KA, Smith AG. 1998. Evidence that the plant host synthesizes the heme moiety of leghemoglobin in root nodules. *Plant Physiology* **116**: 1259–1269.

Schafer A, Tauch A, Jager W, Kalinowski J, Thierbach G, Puhler A. 1994. Small mobilizable multi-purpose cloning vectors derived from the *Escherichia coli* plasmids pK18 and pK19: selection of defined deletions in the chromosome of *Corynebacterium glutamicum*. *Gene* **145**: 69–73.

Shekhawat GS, Verma K. 2010. Haem oxygenase (HO): an overlooked enzyme of plant metabolism and defence. *Journal of Experimental Botany* **61**: 2255–2270.

Shen Q, Jiang M, Li H, Che LL, Yang ZM. 2011. Expression of a *Brassica napus* heme oxygenase confers plant tolerance to mercury toxicity. *Plant, Cell & Environment* **34**: 752–763.

Shimoda Y, Nishigaya Y, Yamaya-Ito H, Inagaki N, Umehara Y, Hirakawa H, Sato S, Yamazaki T, Hayashi M. 2020. The rhizobial autotransporter determines the symbiotic nitrogen fixation activity of *Lotus japonicus* in a host-specific manner. *Proceedings of the National Academy of Sciences, USA* **117**: 1806–1815.

Shoeva OY, Mursalimov SR, Gracheva NV, Glagoleva AY, Börner A, Khlestkina EK. 2020. Melanin formation in barley grain occurs within plastids of pericarp and husk cells. *Scientific Reports* **10**: 1–9.

Suits MD, Pal GP, Nakatsu K, Matte A, Cygler M, Jia Z. 2005. Identification of an *Escherichia coli* O157:H7 heme oxygenase with tandem functional repeats. *Proceedings of the National Academy of Sciences, USA* **102**: 16955–16960.

Tajima S, Takane K, Nomura M, Kouchi H. 2000. Symbiotic nitrogen fixation at the late stage of nodule formation in *Lotus japonicus* and other legume plants. *Journal of Plant Research* **113**: 467–473.

Tripathy BC, Oelmuller R. 2012. Reactive oxygen species generation and signaling in plants. *Plant Signaling & Behavior* **7**: 1621–1633.

VandenBosch KA, Newcomb EH. 1988. The occurrence of leghemoglobin protein in the uninfected interstitial cells of soybean root nodules. *Planta* **175**: 442–451.

Vijayan V, Wagener FADTG, Immenschuh S. 2018. The macrophage heme-heme oxygenase-1 system and its role in inflammation. *Biochemical Pharmacology* **153**: 159–167.

Villafani Y, Yang HW, Park YI. 2020. Color sensing and signal transmission diversity of cyanobacterial phytochromes and cyanobacteriochromes. *Molecules and Cells* **43**: 509–516.

Wang C, Yu H, Luo L, Duan L, Cai L, He X, Wen J, Mysore KS, Li G, Xiao A *et al.* 2016. *NODULES WITH ACTIVATED DEFENSE 1* is required for maintenance of rhizobial endosymbiosis in *Medicago truncatula*. *New Phytologist* **212**: 176–191.

Wang L, Rubio MC, Xin X, Zhang B, Fan Q, Wang Q, Ning G, Becana M, Duanmu D. 2019. CRISPR/Cas9 knockout of leghemoglobin genes in *Lotus japonicus* uncovers their synergistic roles in symbiotic nitrogen fixation. *New Phytologist* **224**: 818–832.

Wang L, Zhou Y, Li R, Liang J, Tian T, Ji J, Chen R, Zhou Y, Fan Q, Ning G *et al.* 2022. Single cell-type transcriptome profiling reveals genes that promote nitrogen fixation in the infected and uninfected cells of legume nodules. *Plant Biotechnology Journal* **20**: 616–618.

Wang LX, Wang LL, Tan Q, Fan Q, Zhu H, Hong Z, Zhang Z, Duanmu D. 2016. Efficient inactivation of symbiotic nitrogen fixation related genes in *Lotus japonicus* using CRISPR-Cas9. *Frontiers in Plant Science* **7**: 1333.

White J, Prell J, James EK, Poole P. 2007. Nutrient sharing between symbionts. *Plant Physiology* **144**: 604–614.

Wilks A, Ikeda-Saito M. 2014. Heme utilization by pathogenic bacteria: not all pathways lead to biliverdin. *Accounts of Chemical Research* **47**: 2291–2298.

Yamaya-Ito H, Shimoda Y, Hakoyama T, Sato S, Kaneko T, Hossain MS, Shibata S, Kawaguchi M, Hayashi M, Kouchi H *et al.* 2017. Loss-of-function of *ASPARTIC PEPTIDASE NODULE-INDUCED 1 (APN1)* in *Lotus japonicus* restricts efficient nitrogen-fixing symbiosis with specific *Mesorhizobium loti* strains. *The Plant Journal* **93**: 5–16.

Yoo SD, Cho YH, Sheen J. 2007. Arabidopsis mesophyll protoplasts: a versatile cell system for transient gene expression analysis. *Nature Protocols* **2**: 1565–1572.

Yu D, Dong Z, Gustafson WC, Ruiz-Gonzalez R, Signor L, Marzocca F, Borel F, Klassen MP, Makhijani K, Royant A *et al.* 2016. Rational design of a monomeric and photostable far-red fluorescent protein for fluorescence imaging *in vivo*. *Protein Science* **25**: 308–315.

Zilli CG, Balestrasse KB, Yannarelli GG, Polizio AH, Santa-Cruz DM, Tomaro ML. 2008. Heme oxygenase up-regulation under salt stress protects nitrogen metabolism in nodules of soybean plants. *Environmental and Experimental Botany* **64**: 83–89.

Supporting Information

Additional Supporting Information may be found online in the Supporting Information section at the end of the article.

Fig. S1 UPLC-MS/MS identification of heme and biliverdin.

Fig. S2 Sequence alignment of the HO1 and HO2 protein families.

Fig. S3 Expression and protein subcellular localization of LjHO2.

Fig. S4 *LjHO1* gene knockout by CRISPR/Cas9.

Fig. S5 Symbiotic phenotypes of *ho1* mutants in Gifu background.

Fig. S6 Characterization of melanin-like pigments of *ho1* brown nodules.

Fig. S7 Symbiotic phenotypes of rhizobial mutants lacking hypothetical heme-degrading enzymes.

Fig. S8 LjHO1 is required for biliverdin production in the plastids of uninfected interstitial cells in Gifu.

Fig. S9 Changes in transcript abundance of leghemoglobin genes (*LjLbs*) in wild-type (WT, MG-20) and *ho1-1* stressed nodules.

Fig. S10 Effect of inhibitors on superoxide and H_2O_2 production in nodules.

Fig. S11 Immunogold localization of leghemoglobins.

Methods S1 Supplemental materials and methods describing construction of rhizobial mutants, determination of heme and biliverdin by UPLC-MS/MS, GUS staining, and expression and purification of recombinant proteins.

Table S1 Primers used in this study.

Please note: Wiley is not responsible for the content or functionality of any Supporting Information supplied by the authors. Any queries (other than missing material) should be directed to the *New Phytologist* Central Office.